**Department of Physics and Astronomy**
**University of Heidelberg**

Bachelor Thesis in Physics
submitted by

**Antonia Schneider**

born in Mannheim (Germany)

**2016**

# Nucleosynthesis in Astrophysical Plasmas

This Bachelor Thesis has been carried out by Antonia Schneider at the
Max Planck Institute for Nuclear Physics in Heidelberg
under the supervision of
PD Adriana Pálffy

**Abstract**

In this work a newly proposed approach to study nuclear reactions relevant for nucleosynthesis under plasma conditions resembling astrophysical sites is investigated from a theoretical point of view. The scheme under investigation makes use of intense optical lasers to accelerate ions via the target normal sheath acceleration scheme. The ions produce nuclear reactions in a second laser-induced target plasma. We describe this process with the help of a fluid model for plasma expansion and take into account the effect of electron screening of the nuclear reaction in the target plasma. In particular, we estimate the neutron yield of the $^{7}$Li(d,n)2$^{4}$He reaction in the laser experimental scenario. This reaction might be the key to explain the remaining lithium production problem of standard big bang nucleosynthesis. The predicted yields show that the $^{7}$Li(d,n)2$^{4}$He reaction in plasma should be observable for the first time in a laboratory experiment under laser parameters available today.

Diese Arbeit beschreibt aus theoretischer Sicht einen neu vorgeschlagenen Ansatz zur Untersuchung von für Nukleosynthese bedeutsamen Kernreaktionen in Plasma unter Bedingungen wie sie in der Astrophysik von Bedeutung sind. Die untersuchte Anordnung nutzt intensive optische Laser zur Beschleuning von Ionen durch den Target-Normal-Sheath-Acceleration-Prozess. Die Ionen verursachen Kernreaktionen in einem zweiten laser-induzierten Plasma. Wir beschreiben diesen Prozess mit Hilfe einens Flüssigkeits-Modells der Ausdehnung von Plasma und berücksichtigen den Elektronen-Abschirm-Effekt in der Kernreaktion im Zielplasma. Insbesondere schätzen wir den Neutronenertrag der Reaktion $^{7}$Li(d,n)2$^{4}$He im Laserexperiment Szenario ab. Diese Reaktion ist möglicherweise von entscheidender Bedeutung zur Erklärung des verbleibenden Lithium-Problems in der standard Big-Bang-Nukleosynthese. Der vorhergesagte Ertrag zeigt, dass die Reaktion $^{7}$Li(d,n)2$^{4}$He in Plasma zum ersten mal in einem Labor Experiment unter heute verfügbaren Laserparametern beobachtbar sein sollte.

# Contents

# Chapter 1

# Introduction

Plasma is the most common form of ordinary matter known, making up over 99% of the visible universe. The intergalactic, interstellar and interplanetary medium as well as solar winds consist mainly of diffuse plasmas while stars are made of dense plasma. In the big bang cosmology the entire universe was a plasma prior to the era of recombination several hundred thousand years after the big bang.
Effects characteristic to the plasma state are therefore important to correctly describe for example the fusion reactions taking place in stars or the nucleosythesis during the early phase of the universe (primordial nucleosnthesis). In this context, one of the most crucial effects is electron screening, meaning that the free electrons in the plasma partially screen the Coulomb barrier between two nuclei, with a resulting enhancement of the fusion reaction rate.

An example of a nuclear reaction in plasma that is important to astrophysics is the $^{7}$Li(d,n)2$^{4}$He reaction. It was recently addressed by Coc et al. [5] as one of the most important reactions affecting the Carbon-Nidrogen-Oxygen (CNO) abundances produced during the big bang nucleosynthesis (BBN). Besides CNO, the $^{7}$Li(d,n)2$^{4}$He reaction rate also influences the Li abundance in the early universe and is therefore interesting in the context of the so-called lithium problem, which describes the disagreement of calculations and measurements of the primordial lithium abundance. Providing new experimental data focused on the determination of the outgoing neutron flux is essential in order to up-grade our knowledge of this process and consequently of the BBN. The critical temperature of about 1GeV will be affordable by the PW laser facility of ELI-NP [9].

The proposed experimental setup is shown in Fig. 1.1. A first laser pulse impinges on a solid $^{7}$Li target of several micrometers thickness. The ultraintense femtosecond laser pulse leads to the appearance of a cloud of hot electrons at the rear surface of the target that accelerates the lithium ions through its electric field. This mechanism is called Target Normal Sheath Acceleration (TNSA). The stream of lithium ions expand along a cone, whose axis is normal to the lithium target surface, and impact on a deuteron plasma. This plasma is generated through the irradiation of a second laser on a deuteron gas jet target. By choosing the duration of the second laser pulse from $10^{-15}$ s up to $10^{-9}$ s one can obtain plasma temperatures ranging from eV to keV [9].

In this thesis we calculate the neutron yield expected for the $^{7}$Li(d,n)2$^{4}$He reaction in such an experiment. We do this for the two cases that the reaction takes place in plasma or in gas.

The thesis has the following structure. First, an introduction into the topic of primordial nucleosyn-

thesis and in particular the so-called lithium problem is given, showing the relevance of the $^{7}$Li(d,n)2$^{4}$He reaction. The next chapter is concerned with cross sections and reaction rates in astrophysics, introducing the concept of the astrophysical S-factor, the Gamow peak and the screening factor. This is followed by a chapter on the model that we use to describe the TNSA mechanism. In the end we present the results of our numerical calculations of the neutron yield from the $^{7}$Li(d,n)2$^{4}$He reaction. The thesis concludes with a Summary and Outlook.

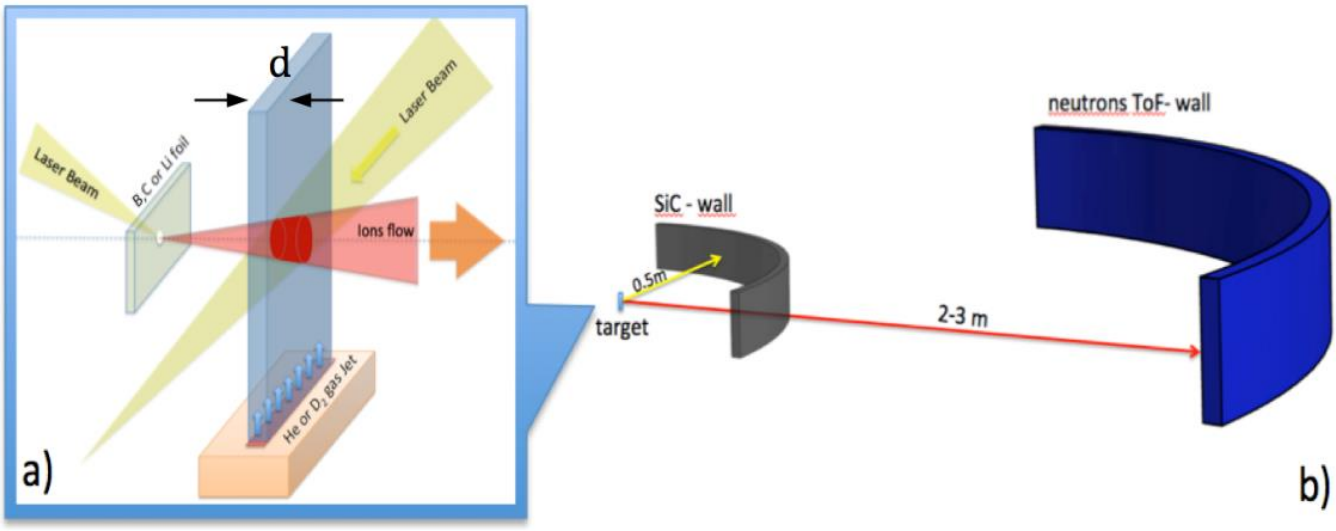


Figure 1.1: experimental setup

# Chapter 2

# Nuclear Reactions in Primordial Nucleosynthesis

Primordial or Big bang nucleosynthesis (BBN) describes the production of the lightest nuclides via a dynamic interplay among the four fundamental forces during the early phases of the universe. The BBN is one of the three evidences for the Big-Bang model together with the expansion of the Universe and the Cosmic Microwave Background (CMB). It is usually assumed to have taken place from $\sim 10$ seconds to $\sim 20$ minutes after the Big Bang when the universe was hot enough for the nuclear reactions in which the lightest stable elements $^4$He, D, $^3$He and $^7$Li were produced to take place [5]. Nuclei heavier than lithium were only produced in comparatively small quantities.

An overview over some of the most important reactions in primordial nucleosynthesis in given in Fig. 2.1.

## 2.1 The Lithium Problem

The primordial abundances of the light elements $^4$He, D and $^7$Li are known from astrophysical observations. In the case of $^4$He one uses He emission lines from nearby metal-poor galaxies. Since $^4$He is produced in stars alongside heavier elements, the primordial abundance (mass fraction) [6]

$$Y_p \approx 0.25$$

is gained through extrapolation to zero metallicity. It is affected by systematic uncertainties such as plasma temperature or stellar absorption.

Deuterium can be measured directly at high redshift. Its most primitive abundance is determined from the observation of distant neutral hydrogen gas clouds, on the line of sight of distant quasars. The measured mass fraction is [6]

$$\left(\frac{\mathrm{D}}{\mathrm{H}}\right)_p = (2.53 \pm 0.04) \cdot 10^{-5}.$$

The primordial lithium abundance is deduced from observations of metall-poor stars in the halo of our Galaxy. In these stars the lithium abundance is almost independent of metallicity, displaying

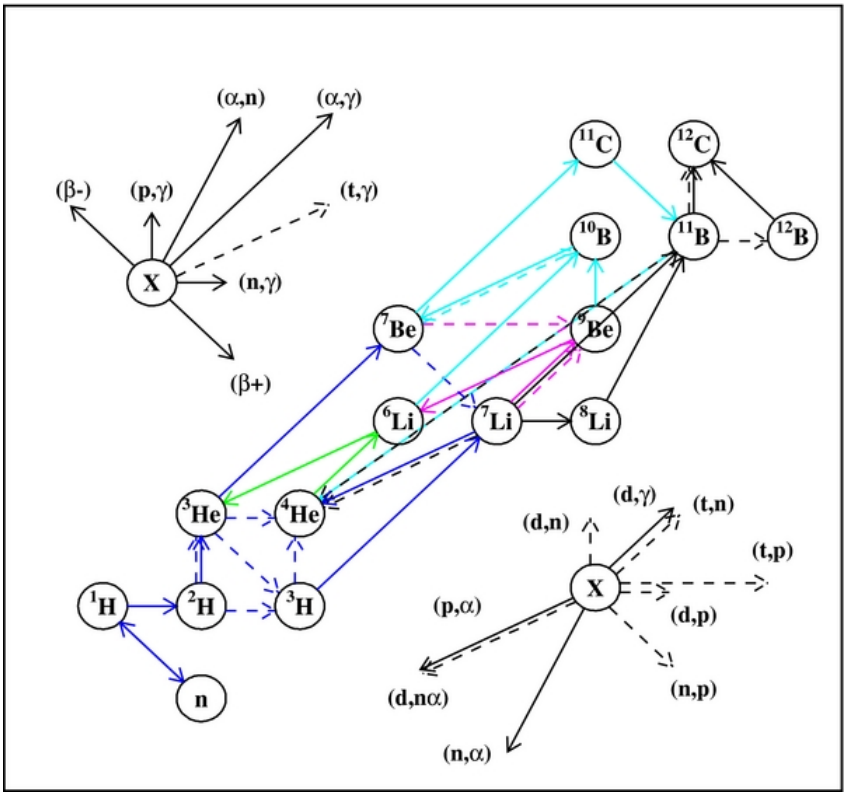


Figure 2.1: Simplified BBN network displaying the important reactions for $^4$He, D, $^3$He, and $^7$Li (blue), $^6$Li (green), $^9$Be (pink), $^{10,11}$B (cyan), and CNO (black) production. Figure taken from Ref. [5]

.

the so-called Spite plateau (see Fig. 2.2). Because heavy elements (metals) increase with time as Galactic nucleosynthesis proceeds, this plateau indicates that the lithium abundance in these stars is unrelated to Galactic nucleosynthesis processes and thus is primordial [8]. This gives [6]

$$\left(\frac{\mathrm{Li}}{\mathrm{H}}\right)_p = (1.6 \pm 0.3) \cdot 10^{-10}.$$

These observations can be compared to the predictions of the standard BBN, which is a theory of light-element production combining the Standard Model of particle physics with the standard cold dark matter cosmology [8]. All the parameters that enter into standard BBN have been measured today. The number of light neutrino families, the lifetime of the neutron important to weak reaction rate calculations and many nuclear reaction rates have been measured in laboratories. In standard BBN, the abundances are usually parameterised by the baryon-to-photon ratio $\eta \equiv n_b/n_\gamma$, or equivalently the present baryon density $\Omega_b h^2 \equiv \omega_b$. This quantity has been fixed by a series of precise measurements of cosmic microwave background (CMB) anisotropies, for example by the Wilkinson Microwave Anisotropy Probe (WMAP) [5] and most recently by the Planck space telescope [6] yielding

$$\eta = 6.10 \pm 0.04,$$

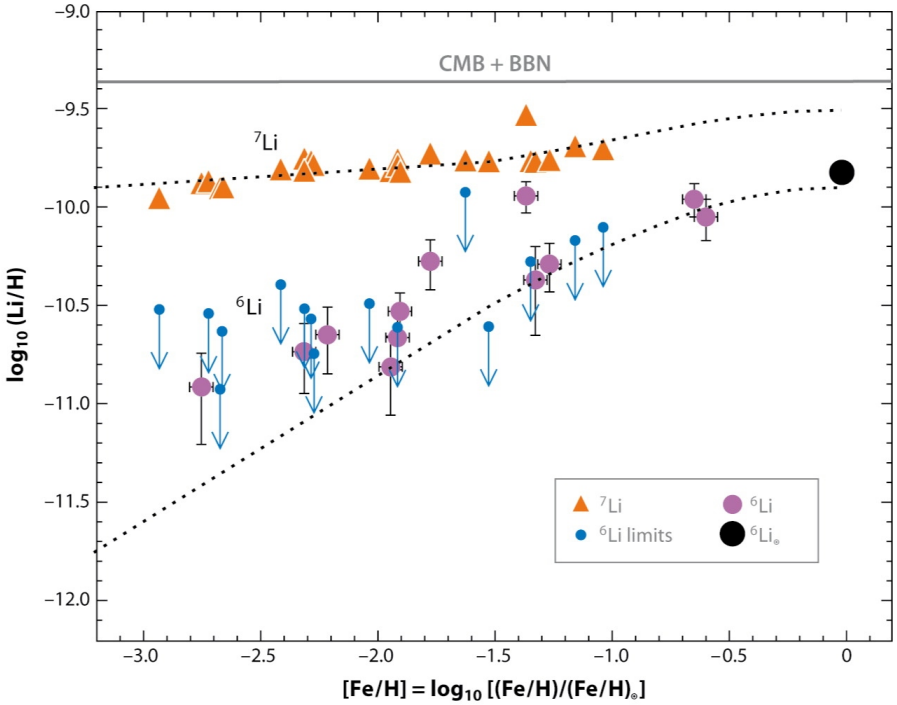


Figure 2.2: Lithium abundances versus the star's metallicity in selected metal-poor Galactic halo stars. The horizontal band gives the CMB prediction; the gap between this prediction and the plateau illustrates the $^7$Li problem. Figure taken from Ref. [8].

$$\omega_b = 0.02225 \pm 0.00016.$$

The abundance of several elements at times up to $10^4$ s as predicted by standard BBN using the parameters named above, is depicted in Fig. 2.5.

There is an overall agreement between predictions by the standard BBN using the CMB baryon density and observations of light element abundances, except for $^7$Li (see Fig. 2.3). This phenomenon is known as the lithium problem. Any model that tries to solve the lithium must reduce $^7$Li abundance substantially, yet not perturb the other light elements unacceptably. There are three categories of possible solutions to the lithium problem [8]:

(1) systematic uncertainties in astrophysical measurements of the lithium abundance and/or their interpretation

(2) revised nuclear physics inputs to the BBN calculation, in the form of increased $^7$Li destruction via novel reaction pathways or by resonant enhancement of otherwise minor channels

(3) new physics beyond the Standard Model of particle physics or large changes to the cosmological framework used to interpret light-element data

The $^7$Li(d,n)2$^4$He rate is an important input into the standard BBN calculation of the lithium abundance. The measurement of this rate under extreme plasma conditions, as in the experiment discussed in this thesis, can therefore contribute to the second category named above. The effect of increasing the

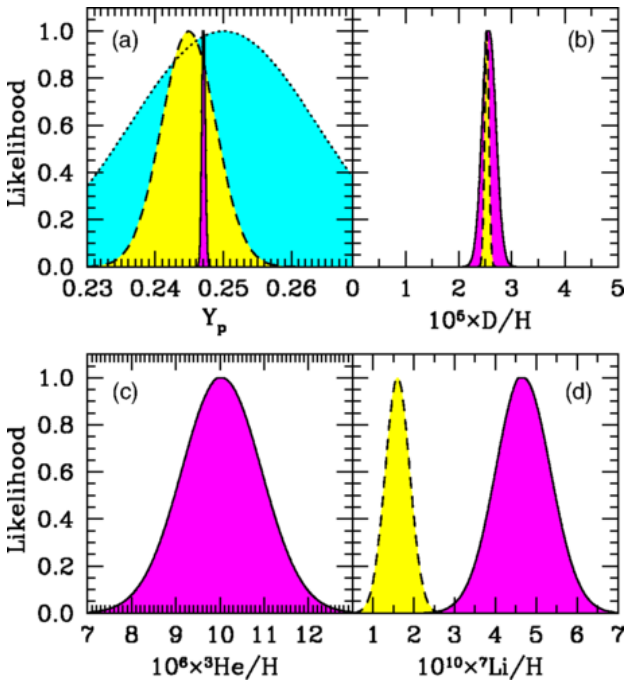


Figure 2.3: Light-element predictions using the CMB determination of the cosmic baryon density. The purple curves are the BBN+CMB predictions. The yellow curves show astronomical measurements of the primordial abundances, for all but $^3$He where reliable primordial abundance measures do not exist. The cyan curve shows the CMB determination of $^4$He. Figure from Ref. [6].

$^7$Li(d,n)2$^4$He reaction rate by a factor of 1000 is depicted in Fig. 2.4. Even though the final abundances are left unchanged, the peak $^7$Li abundance at $t \approx 200$s is reduced by a factor of about 100.

The sensitivity study in Ref.[5] has furthermore shown that the reaction $^7$Li(d,n)2$^4$He has a considerable effect on the Carbon-Nitrogen-Oxygen (CNO) nucleosynthesis. How a changed rate of the $^7$Li(d,n)2$^4$He reaction would influence the primitive CNO abundance according to Ref. [5] is shown in Table 2.1.

| $f$ | 0.001 | 0.01 | 0.1 | 10 | 100 | 1000 |
|---|---|---|---|---|---|---|
| $X_i/X_{i0}$ | 1.66 | 1.65 | 1.55 | $2.80 \cdot 10^{-1}$ | $5.99 \cdot 10^{-1}$ | $2.18 \cdot 10^{-2}$ |

Table 2.1: Ratio of the standard BBN abundance $X_i0$ of CNO and the abundance $X_i$ when the reaction rate of $^7$Li(d,n)2$^4$He is changed by factor $f$.

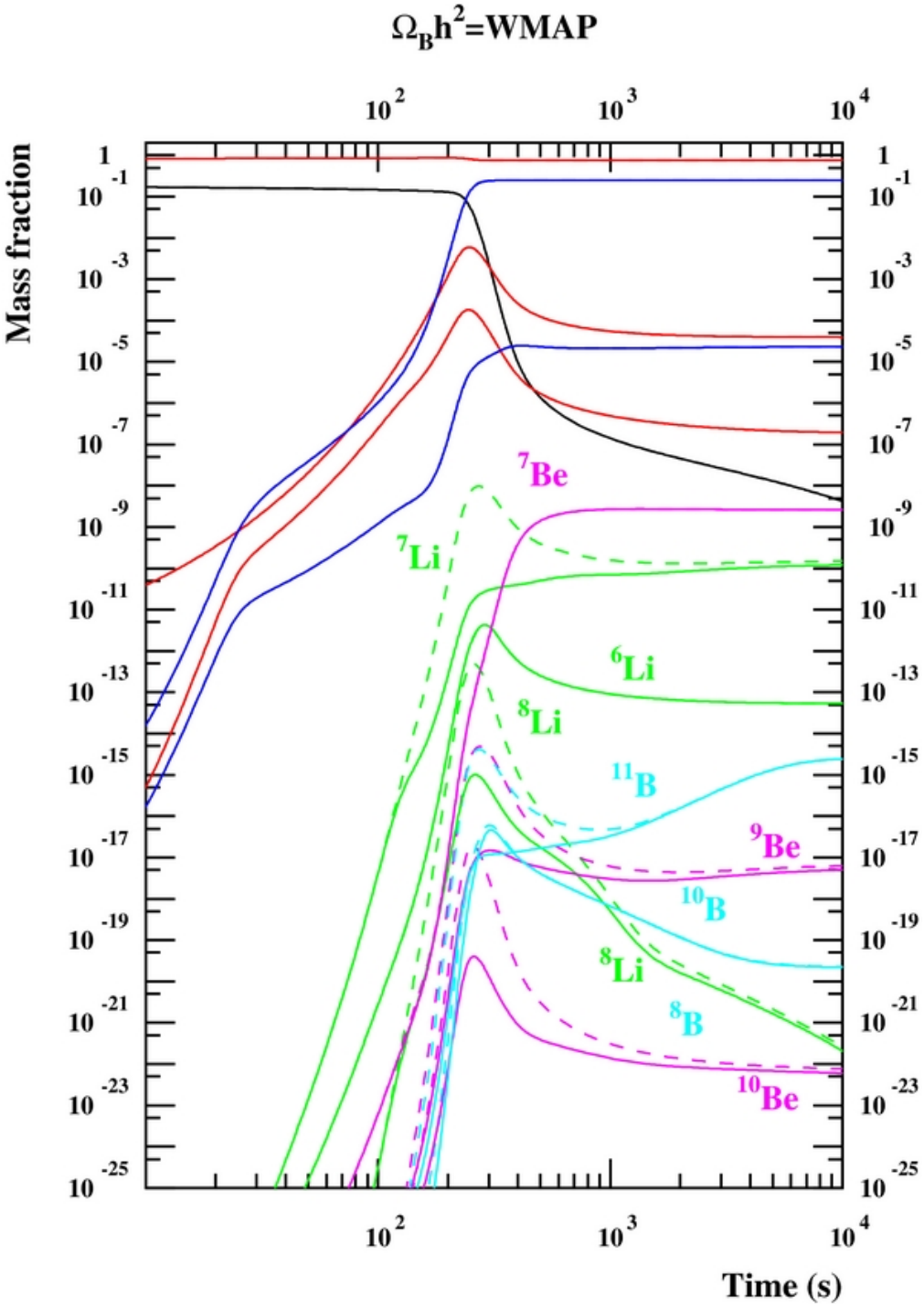


Figure 2.4: Standard big bang nucleosynthesis production of H, He, Li, Be, and B isotopes with the $^{7}$Li(d,n)2$^{4}$He reaction rate from Ref. [4] (dashed lines) and with the same rate multiplied by a factor of 1000 (solid lines). $\Omega_b h^2$ = WMPA means that the baryon density for this calculation taken from WMAP. Figure from Ref. [5]

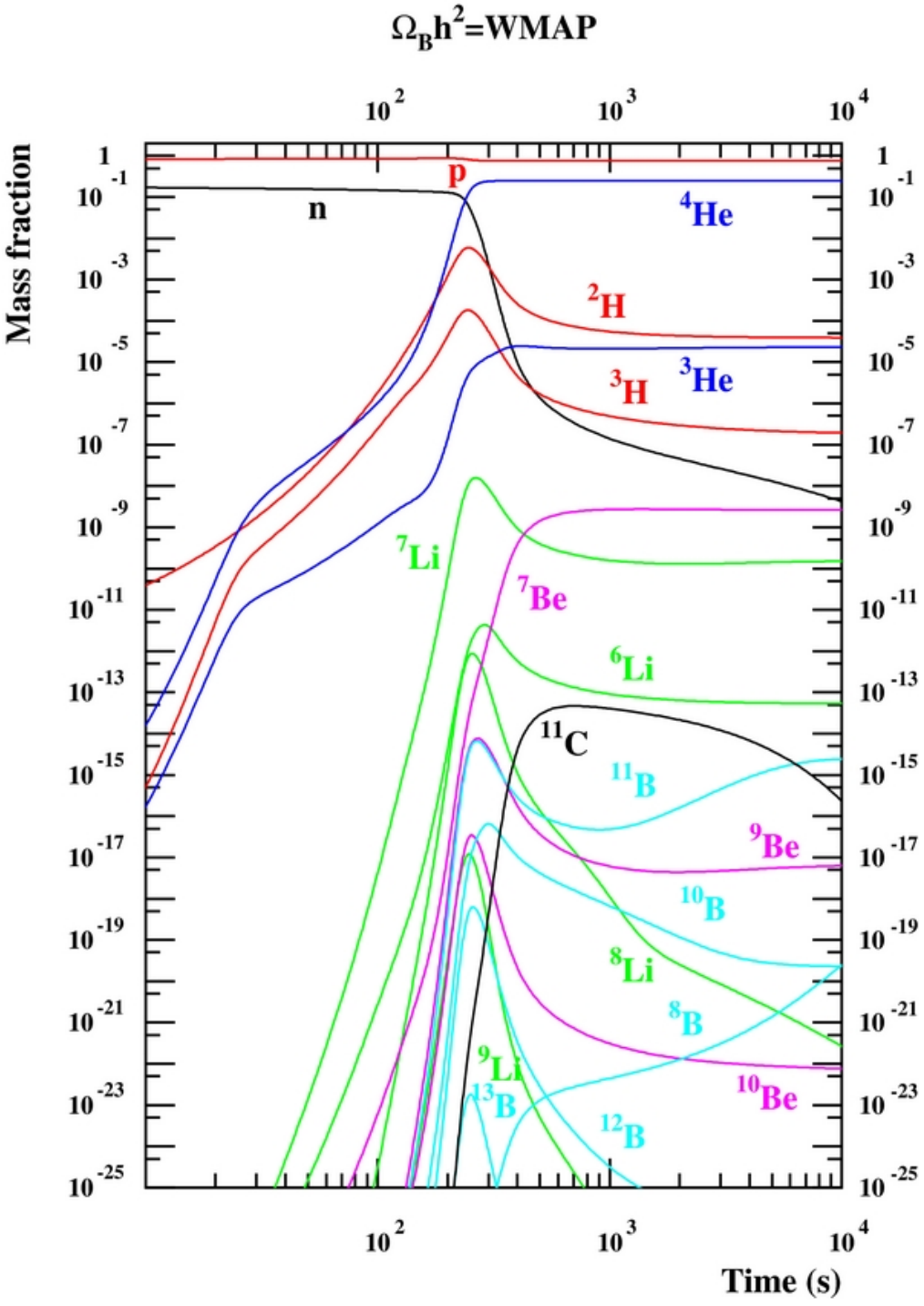


Figure 2.5: Standard BBN production of different elements as a function of time. $\Omega_b h^2 =$ WMPA means that the baryon density for this calculation taken from WMAP. Figure from Ref. [5]

# Chapter 3

# Reaction Rate in Plasmas

The center of mass energy of two colliding nuclei with the reduced mass $\mu = m_1 m_2/(m_1 + m_2)$ and relative velocity $v = v_1 - v_2$ is

$$E = \frac{1}{2}\mu v^2. \tag{3.1}$$

The cross section $\sigma$ for a reaction is an area that describes the probability of a pair of nuclei to react. Classically, the geometrical cross section is equal to the combined geometrical area $\pi(r_1 + r_2)^2$ of the projectile with radius $r_1$ and the target with radius $r_2$. In quantum mechanics, the sum of radii has to be replaced by the reduced de Broglie wavelength, so that the geometrical cross section is inversely proportional to the center-of-mass energy of the reaction [1]

$$\sigma_{\text{geom}} \propto \lambda^2 = \left(\frac{h}{\mu v}\right)^2 \propto \frac{1}{E}. \tag{3.2}$$

In order to fuse, the nuclei have to overcome the Coulomb potential

$$V_C(r) = Z_1 Z_2 e^2 r^{-1} \tag{3.3}$$

at nuclear radius $r = r_n$, where the strong and attractive nuclear force comes into play. Since one can assume $E \ll V_C(r_n)$, the cross section is proportional to the probability $P$ of a nucleus tunneling the Coulomb barrier. For energy $E = V_C(r_c)$ the classical turning point is $r_c$ and the probability $P$ of barrier penetration (tunneling) is therefore given by the ratio of the square of the wave function $\Psi$ at distances $r_n$ and $r_c$

$$\sigma \propto P = \frac{|\Psi(r_n)|^2}{|\Psi(r_c)|^2}. \tag{3.4}$$

Solving the Schrödinger equation delivers [18]

$$P = \exp\left[-2K r_c \left(\frac{\arctan(r_c/r_n - 1)^{0.5}}{(r_c/r_n - 1)^{0.5}}\right) - \frac{r_n}{r_c}\right] \tag{3.5}$$

with $K = \sqrt{2\mu(V_C(r_n) - E)}\hbar^{-1}$. At low energies $E \ll V_C(r_n)$, that is $r_n \ll r_c$, one can approximate

Eq. (3.5) as follows

$$P = \exp(-2\pi\eta);\ \eta = Z_1 Z_2 e^2 \alpha \sqrt{\frac{\mu}{2E}}. \tag{3.6}$$

The parameter $\eta$ is called the Sommerfeld parameter and $\alpha$ is the fine-structure constant. Alternatively, $P$ can be expressed in terms of the Gibbs energy $E_G$,

$$P = \exp\left(-\sqrt{\frac{E_G}{E}}\right);\ E_G = (Z_1 Z_2 \alpha\pi)^2 \mu c^2. \tag{3.7}$$

Combining Eq. (3.2) and Eq. (3.4) leads to the cross section

$$\sigma(E) = \frac{S(E)}{E} \exp(-2\pi\eta), \tag{3.8}$$

here $S(E)$ is the astrophysical factor, which contains the strictly nuclear effects of the reaction after barrier penetration. For non-resonant reactions, $S(E)$ varies smoothly and much less rapidly with energy than the cross section does. It is therefore a useful quantity if one wants to extrapolate data to low energies.

The reaction rate per particle pair is the product of the cross section and the relative velocity averaged over all velocities

$$< \sigma v >= \int_0^\infty \Phi(v)\, \sigma(v) v \, \mathrm{d}v, \tag{3.9}$$

where the function $\Phi(v)$ gives the probability of the relative velocity being $v$ and fulfills $\int_0^\infty \Phi(v)\, \mathrm{d}v = 1$. The number of reactions per volume and time between nuclei of species x and y with densities $n_x$ and $n_y$ is then given by

$$R = n_x n_y \left(1 + \delta_{xy}\right)^{-1} < \sigma v > . \tag{3.10}$$

Without the Kronecker delta $\delta_{xy}$ all reactions would be counted twice if the nuclei are of the same species. In thermodynamic equilibrium the velocities of both nuclei follow a Boltzmann distribution and Eq. (3.9) turns into [18]

$$< \sigma v >= \sqrt{\frac{8}{\pi\mu}} (k_B T)^{-3/2} \int_0^\infty \exp\left(-\frac{E}{k_B T}\right) E\ \sigma(E)\, \mathrm{d}E. \tag{3.11}$$

Inserting the cross section from Eq. (3.8) into Eq. (3.11) leads to

$$< \sigma v > \propto \int_0^\infty S(E) \exp\left(-\frac{E}{k_B T} - \sqrt{\frac{E_G}{E}}\right) \mathrm{d}E. \tag{3.12}$$

Because $S(E)$ varies relatively slowly with energy, the energy dependence of the integrand in Eq. (3.12) is dominated by the two exponential terms. The Boltzmann factor vanishes at high energy and the barrier penetrability goes to zero at low energy so that the product of both leads to a peak (so-called Gamow peak) of the integrand at energy $E_p = (\sqrt{E_G} k_B T/2)^{\frac{2}{3}}$ [18]. This formula is widely used in order to determine the effective energy region in which most of the nuclear reactions occur at given temperature.

## 3.1 Screening Effect

The electrostatic potential of an ion in a plasma causes a polarization in the surrounding electrons and nuclei so that part of the ion charge is shielded by a cloud of free electrons. The Coulomb barrier that two reacting nuclei have to overcome is therefore lowered and the nuclear reaction rate increased. This is called the screening effect.

At temperatures and densities relevant to primordial nucleosynthesis the screening is weak, that is the Coulomb interaction energy between a nucleus and the surrounding charge cloud is small compared to the thermal energy.

We now derive the screening factor for the the case of weak screening following the description in Ref. [20].

We can assume all atoms to be completely ionized: The ratio of the ionization potential of a K-shell electron in a hydrogen-like atom of charge $Z$ to the mean thermal energy is

$$I_z = \frac{1}{4\pi\epsilon_0}\frac{Ze^2}{2a_0}\frac{1}{k_B T} \ll 1, \tag{3.13}$$

where $a_0 = 4\pi\epsilon_0\hbar^2/m_e Ze^2$ is the Bohr radius for such an atom.

The reaction rate in the plasma of temperature $T$ is proportional to

$$\int_0^\infty \left[\sqrt{E}\exp\left(-\frac{E}{k_B T}\right)\right] P(E)\,\sigma_{\text{nuc}}(E)\,\mathrm{d}E. \tag{3.14}$$

The term in square brackets in this integrand is the Maxwell-Boltzmann factor, $P$ is the barrier penetration factor and $\sigma_{\text{nuc}}$ the nuclear factor. The latter depends on the details of the interaction after barrier penetration.

Two colliding nuclei of charge $Z_1$ and $Z_2$ each carry a cloud of free electrons with them through the plasma, screening part of their charge. Therefore, the total interaction energy between the two nuclei at distance $r_{12}$ can be written as

$$U_{tot}(r_{12}) = Z_1 Z_2 e^2/r_{12} + U(r_{12}). \tag{3.15}$$

The integrand of Eq. (3.14) has a sharp maximum at the energy $E_{max} >> k_B T$. Let $r_n$ be the nuclear radius and $r_c$ the classical turning point at energy

$$E_{max} = \frac{Z_1 Z_2 e^2}{r_c}. \tag{3.16}$$

We define the parameter $a$ as the average inter-particle distance given by

$$4\pi a^3 \rho N_A = 1, \tag{3.17}$$

where $\rho$ is the density in $\mathrm{g\,cm^{-3}}$ and $N_A$ the Avogadro number.The charge cloud surrounding a nucleus has radius $R > a$.

We assume $r_c \ll R$. $P$ essentially only depends on $U_{tot}$ for distances $r_{12}$ between $r_n$ and $r_c$. $U(r_{12})$

must be small for $r_{12} \gg R$ and approach a constant value $U_0 \sim Z_1 Z_2 e^2/R$ as $r_{12}$ becomes small compared with $R$. It follows that

$$\frac{r_c}{R} \sim \frac{U_0}{E_{max}} \ll 1. \tag{3.18}$$

Because $U(r)$ is only needed for $r_{12} \ll r_c$ it can be replaced by a constant potential $U_0 = U(r=0)$. The penetration factor $P$ and nuclear factor $\sigma_{nuc}$ without electron screening at energy $E$ are then equal to the correct factors with screening at an energy $E + U_0$. Therefore, Eq. (3.14) turns into

$$\int_0^\infty \sqrt{E+U_0} \exp\left(-\frac{E+U_0}{k_B T}\right) P(E)\, \sigma_{nuc}(E)\, \mathrm{d}E. \tag{3.19}$$

Since $E_{max} \gg U_0$ we can assume $\sqrt{E+U_0} \approx \sqrt{E}$. With these approximations the effect of electron screening on the reaction rate is expressed by the factor

$$g_{scr} = \exp\left(-\frac{U_0}{k_B T}\right) \tag{3.20}$$

with $U_0 = Z_1 Z_2 e^2/R$.

In order to find an expression for $R$, we first write the interaction energy between nuclei of charges $Z_1$ and $Z_2$ at distance $r$ in the following form

$$U_{tot}(r) = Z_1 Z_2 e^2 \Psi_{tot}(r);\ \Psi_{tot}(r) = r^{-1} + \Psi(r). \tag{3.21}$$

The charge $Z_1$ is fixed at $r = 0$. We introduce the electrostatic potential $V(r) = Z_1 e \Psi(r)$ and the electric charge density $\bar{\rho}(r)$, which are averaged over all particles except the nucleus at the origin $r = 0$. They are related via the Poisson equation:

$$\nabla^2[Z_1 e \Psi_{tot}(r)] = -4\pi\bar{\rho}(r) - 4\pi Z_1 e \delta^{(3)}(r). \tag{3.22}$$

Let $z$ and $A$ be the charge and mass number of the main constituent of the gas. Taking into account the Boltzmann factors of electrons and nuclei, the charge density is

$$\bar{\rho}(r) = \frac{\rho N_A z e}{A} \exp\left[\frac{-Z_1 z e^2 \Psi_{tot}(r)}{k_B T}\right] - \exp\left[\frac{Z_1 z e^2 \Psi_{tot}(r)}{k_B T}\right]. \tag{3.23}$$

In the case of weak screening the two exponential factors in Eq. (3.22) are small for $r$ in the order of magnitude of $a$ or larger. Expanding those exponential factors and substituting Eq. (3.23) into Eq. (3.22) gives

$$\nabla^2 \Psi(r) = 4\pi\rho N_A \frac{z^2+z}{A} \frac{e^2}{k_B T}\left[\frac{1}{r} + \Psi(r)\right]. \tag{3.24}$$

The solution of Eq. (4.5) is

$$\Psi(r) = r^{-1}(\exp[-r/R] - 1);\ \Psi(0) = -R^{-1}, \tag{3.25}$$

with

$$R = \left(\frac{k_B T}{4\pi\rho N_A e^2}\right)^{\frac{1}{2}} \zeta^{-1} = \left(\frac{k_B T}{e^2/a}\right)^{\frac{1}{2}} a^2 \zeta^{-1}, \tag{3.26}$$

and

$$\zeta = \sqrt{\frac{z^2 + z}{A}}. \tag{3.27}$$

Inserting Eq. (3.26) into Eq. (3.20) gives the screening factor for weak screening if one assumes that the electrons are non-degenerate. Non-degeneracy means that the ratio of Fermi energy and thermal energy $D = E_F/k_B T$ is much smaller than one. For non-relativistic electrons, the Fermi energy is

$$E_F = \frac{\hbar^2}{8\pi^2 m}(3\pi^2 N_A \xi \rho)^{\frac{2}{3}}, \tag{3.28}$$

with the the average number of electrons per atomic mass unit

$$\xi = \sum_i \frac{x_i z_i}{A_i}, \tag{3.29}$$

where $x_i$ is the fractional abundance by mass of nuclei of charge $z_i$ and mass $A_i$.

We now consider weak screening in case of an arbitrary degree of electron degeneracy, that is an arbitrary ratio $D = \frac{E_F}{k_B T}$. Let $f(\eta)$ be the Fermi-Dirac function,

$$f(\eta) = \int_0^\infty \sqrt{x}\,[\exp(x - \eta)]^{\frac{1}{2}}\,\mathrm{d}x. \tag{3.30}$$

If the electrons at point $r$ experience the interaction energy $U_e$, the ratio of the actual density and the field-free density is $f(\eta - U_e/k_B T)/f(\eta)$, where $f'$ is the derivative of $f$ and $\eta$ is given by $f(\eta) = \frac{2}{3}D^{\frac{3}{2}}$. If $a < r \sim R$ then $U_e \ll k_B T$ for weak screening. With a Taylor expansion of $f(\eta - U_e/k_B T)$ up to the second term, the ratio of actual density to field free density becomes

$$\frac{f(\eta - U_e/k_B T)}{f(\eta)} = 1 - \frac{f'(\eta)}{f(\eta)} \cdot \frac{U_e(r)}{k_B T}. \tag{3.31}$$

This gives the general form of the quantity $\zeta$ from Eq. (3.26)

$$\zeta = \left[\sum_i x_i \frac{z_i^2}{A_i} + \left(\frac{f'}{f}\right)\sum_i x_i \frac{z_i}{A_i}\right]^{\frac{1}{2}}. \tag{3.32}$$

Thus, the final result for the screening factor in a weakly screened plasma is

$$g_{scr} = \exp\left(\frac{Z_1 Z_2 e^2}{R \cdot k_B T}\right), \tag{3.33}$$

with $R$ from Eq. (3.26) and $\zeta$ from Eq. (3.32). We will therefore multiply our calculated number of neutrons resulting from the reaction $^7$Li(d,n)2$^4$He with this screening factor to take into account that the reaction is taking place in a plasma.

# Chapter 4

# Target Normal Sheath Acceleration

Let us assume in the following a scenario in which a strong, PW laser hits on a solid-state target composed of light-Z elements. The laser irradiation generates a current of hot electrons at the front side of the target that eventually reaches the rear side. There, as the hot electrons attempt to escape out of the target, the charge unbalance generates a sheath field normal to the rear surface that accelerates the ions. This scheme is known as Target Normal Sheath Acceleration (TNSA). TNSA was intensively studied in the last years; experiments and models show that this acceleration scheme works very well in the intensity domain between $10^{18} - 10^{20}\,\mathrm{W\,cm^{-2}}$ [17, 13].

In this section, we introduce a model describing the TNSA scheme that is based on the fluid model of plasma expansion into a vacuum studied in Ref. [15]. The model from Ref. [15] is an isothermal, fluid model, in which the charge separation effects in the collisionless plasma expansion can be studied. In this model, at time $t = 0$, a plasma is assumed to occupy the half-space $x < 0$. The ions are cold and initially at rest with density $n_i = n_{i0}$ for $x < 0$ and $n_i = 0$ for $x > 0$ with a sharp boundary. The electron density $n_e$ is continuous and corresponds to a Boltzmann distribution

$$n_e = n_{e0} \exp\left(\frac{e\Phi}{k_B T_e}\right), \tag{4.1}$$

where $T_e$ is the electron temperature, $\Phi$ the electrostatic potential and $e$ the electron charge. We assume quasi-neutrality $n_e = Z n_i$ in the plasma.

The potential $\Phi$ is described by the Poisson equation

$$\epsilon_0 \partial^2 \Phi / \partial x^2 = e(n_e - Z n_i), \tag{4.2}$$

and the initial condition $\Phi(-\infty) = 0$.

The ion velocity $v_i$ is then given by the equations of continuity and motion:

$$(\partial/\partial t + v_i \partial/\partial x) n_i = -n_i \partial v_i / \partial x, \tag{4.3}$$

$$(\partial/\partial t + v_i \partial/\partial x) v_i = -(Ze/m_i) \partial \Phi / \partial x. \tag{4.4}$$

For times $x + c_s t > 0$, Eqs. (4.1), (4.2),(4.3) and (4.4) are solved by the the self-similar expansion

$$n_e = Z_i n_i = n_{e0} \exp\left(-\frac{x}{c_s t} - 1\right), \tag{4.5}$$

$$v_i = c_s + \frac{x}{t}, \tag{4.6}$$

and the corresponding self-similar electric field

$$E_{ss} = \frac{k_B T_e}{e c_s t}. \tag{4.7}$$

In the equations above, $m_i$ is the ion mass and $c_s$ is the ion sound speed,

$$c_s = \sqrt{\frac{Z k_B T_e}{m_i}}. \tag{4.8}$$

Based on the self-similar expansion [Eqs. (4.5)- (4.7)] and numerical solutions of Eqs. (4.1)- (4.4), Mora obtained in Ref. [15] a very good approximation for the electric field at the ion front,

$$E_{\text{front}}(t) = 2\sqrt{n_{e0} k_B T / \epsilon_0} \frac{1}{\sqrt{2\exp(1) + \omega_{pi}^2 t^2}}. \tag{4.9}$$

This equation is compared to experimental results in Fig. 4.2.

Integrating $\frac{d}{dt} v_{\text{front}} = Z e E_{\text{front}} / m_i$ gives the velocity of the ion front

$$v_{\text{front}}(t) \approx 2 c_s \ln(\tau + \sqrt{\tau^2 + 1}), \tag{4.10}$$

where the ion plasma frequency $\omega_{pi} = \sqrt{n_{e0} Z k_B T_e / m_i}$ is used to normalize the time

$$\tau = \frac{\omega_{pi} t}{\sqrt{2\exp(1)}}. \tag{4.11}$$

The charge distribution resulting from this model can be seen in Fig. 4.3 at time $\omega_{pi} t = 50$. There are two layers of positive surface charge density, one around the position $x = -c_s t$ and a second one just on the left of the ion front. Just right of the ion front there is an electron cloud with charge density $\sigma = -\epsilon_0 E_{ss}$.

The fluid model from Ref. [15] is isothermal and would thus predict endless ion acceleration. To take into account the progressive transfer of energy from the fast electrons to the ions one may therefore introduce a phenomenological maximum acceleration time $t_{\text{acc}}$ depending on the laser pulse duration $\tau_{\text{laser}}$. According to Ref. [10], the approximation $t_{\text{acc}} \sim 1.3\tau_{\text{laser}}$ matches well with experimental results.

Using Eq. (4.10), the maximum (cutoff) energy of the ions is then

$$E_{max} = \frac{m_i}{2} v_{\text{front}}^2 (t = t_{acc}) = 2 Z_1 k_B T_e \left[\ln\left(t_p + \sqrt{t_p^2 + 1}\right)\right]^2, \tag{4.12}$$

where $t_p$ is the normalized acceleration time

$$t_p = \frac{\omega_{pi} t_{\mathrm{acc}}}{\sqrt{2\exp(1)}}. \tag{4.13}$$

In most of the experiments, a preformed plasma (preplasma) is present in front of the target owing to the long-duration, low-level laser energy reaching the target before the main pulse. The electrons are accelerated into the target following the irradiation by the main pulse. As the electrons are accelerated over the laser pulse duration and spread over the surface of the sheath $S_{\mathrm{sheath}}$, one has

$$n_{e0} = \frac{N_e}{c\,\tau_{\mathrm{laser}} S_{\mathrm{sheath}}}, \tag{4.14}$$

where $N_e$ is the total number of electrons. The surface of the sheath $S_{\mathrm{sheath}}$ is given as

$$S_{\mathrm{sheath}} = \pi(r_0 + d\tan\theta)^2. \tag{4.15}$$

The quantity $S_{\mathrm{sheath}}$ depends on the half-angle divergence ($\theta \sim 25\,^\circ$) of the hot electron inside the target [10], the target thickness $d$ and the initial radius $r_0$ of the zone over which the electrons are accelerated at the target front surface, that is, the laser spot. For given laser power $P$ and laser intensity $I$ this radius can be calculated via

$$r_0 = \sqrt{\frac{P}{\pi I}}. \tag{4.16}$$

The model predicts a number of accelerated ions per energy and surface given by [10]

$$\frac{dN}{dE} = \frac{n_{i0} c_s t_{\mathrm{acc}} S_{\mathrm{sheath}}}{\sqrt{2EE_0}} \exp\left(-\sqrt{\frac{2E}{E_0}}\right), \tag{4.17}$$

with $E_0 = Zk_B T_e$.

In order to obtain the cutoff energy and the energy spectrum of the ions, the density $n_{e0}$ and temperature $T_e$ of the electrons must be known. The electron temperature is found numerically [23] and experimentally [14] to be given by the laser ponderomotive potential,

$$k_B T_e = m_e c^2 \left[\sqrt{1 + \frac{I\lambda^2}{1.37\cdot 10^{18}}} - 1\right], \tag{4.18}$$

where $m_e$ is the electron mass, $I$ is the laser intensity in $\mathrm{W\,cm^{-2}}$, and $\lambda$ is the laser wavelength in micrometers. As shown in Ref. [10], the total number of electrons accelerated into the target is

$$N_e = \frac{f E_{\mathrm{laser}}}{k_B T_e}, \tag{4.19}$$

where $E_{\mathrm{laser}}$ is the laser energy and $f$ is the fraction of laser light that is absorbed into the preplasma. According to a recent fit of experimental results, the following dependence of the fraction $f$ on the laser

intensity can be adopted [22, 7, 11]

$$f = \left( \frac{I\lambda^2}{4.3 \cdot 10^{21}\ \mathrm{W}\frac{\mu\mathrm{m}^2}{\mathrm{cm}^2}} \right)^{0.2661} . \tag{4.20}$$

This fit was shown to be adequate from $2 \cdot 10^{18}$ to $2 \cdot 10^{20}$ $\mathrm{W}\,\mu\mathrm{m}^2\,\mathrm{cm}^{-2}$ ; beyond $2 \cdot 10^{20}$ $\mathrm{W}\,\mu\mathrm{m}^2\,\mathrm{cm}^{-2}$ the absorption is leveling off or even falling [7].
Fig. 4.4 shows that the TNSA model described above fits quite well the experimental results. We will use this model to calculate the energy spectrum of the Lithium ions that were accelerated by laser irradiation on the primary target.

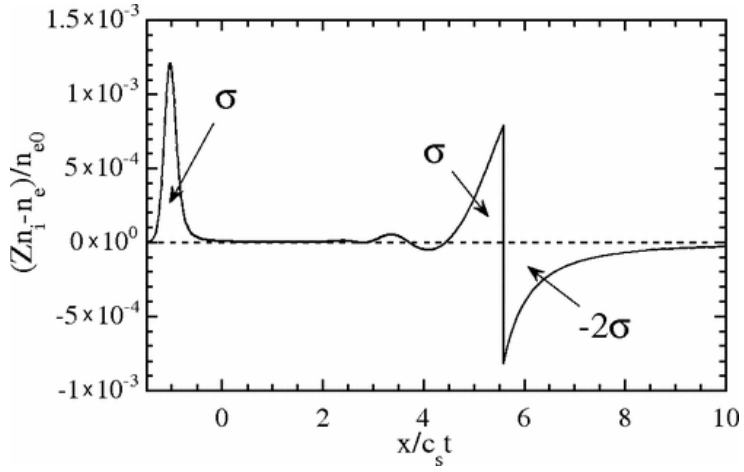


Figure 4.1: Charge density at time $\omega_{pi}t = 50$ Figure from Ref. [15].

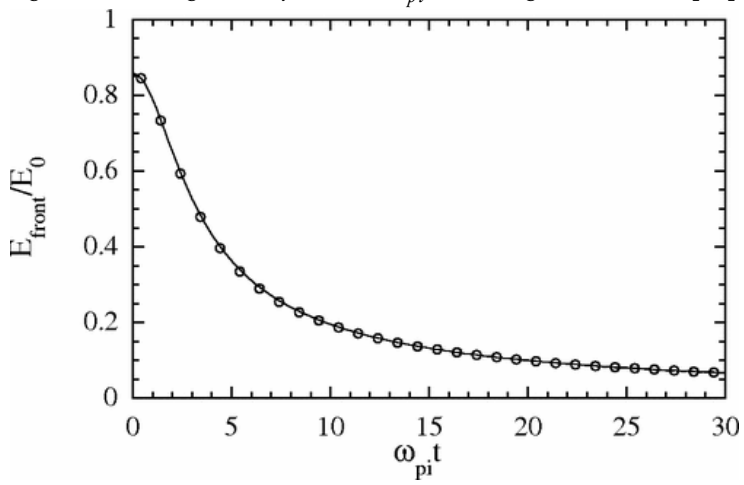


Figure 4.2: Electric field at the ion front as a function of time. The empty circles correspond to the numerical results and the full line to the theoretical formula [Eq. (4.9)]. Figure from Ref. [15].

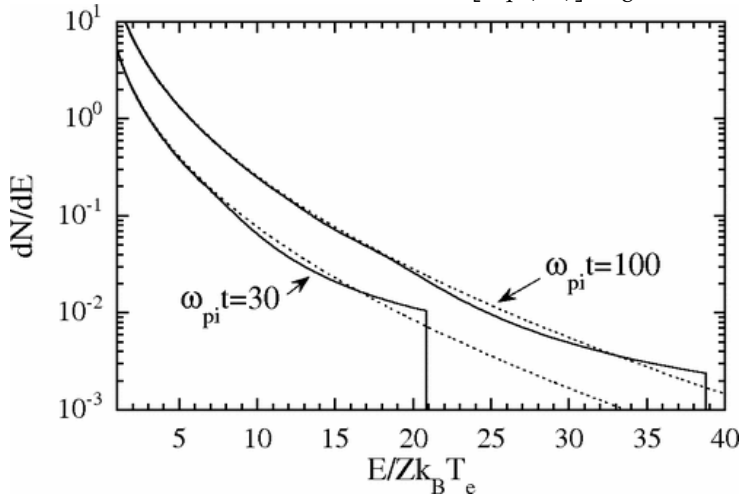


Figure 4.3: Energy spectrum per unit surface as a function of the energy normalized to $Zk_BT_e$. The dotted lines correspond to the prediction of the self-similar solution [Eq. (4.17)] and the full line to numerical results. Figure from Ref. [15].

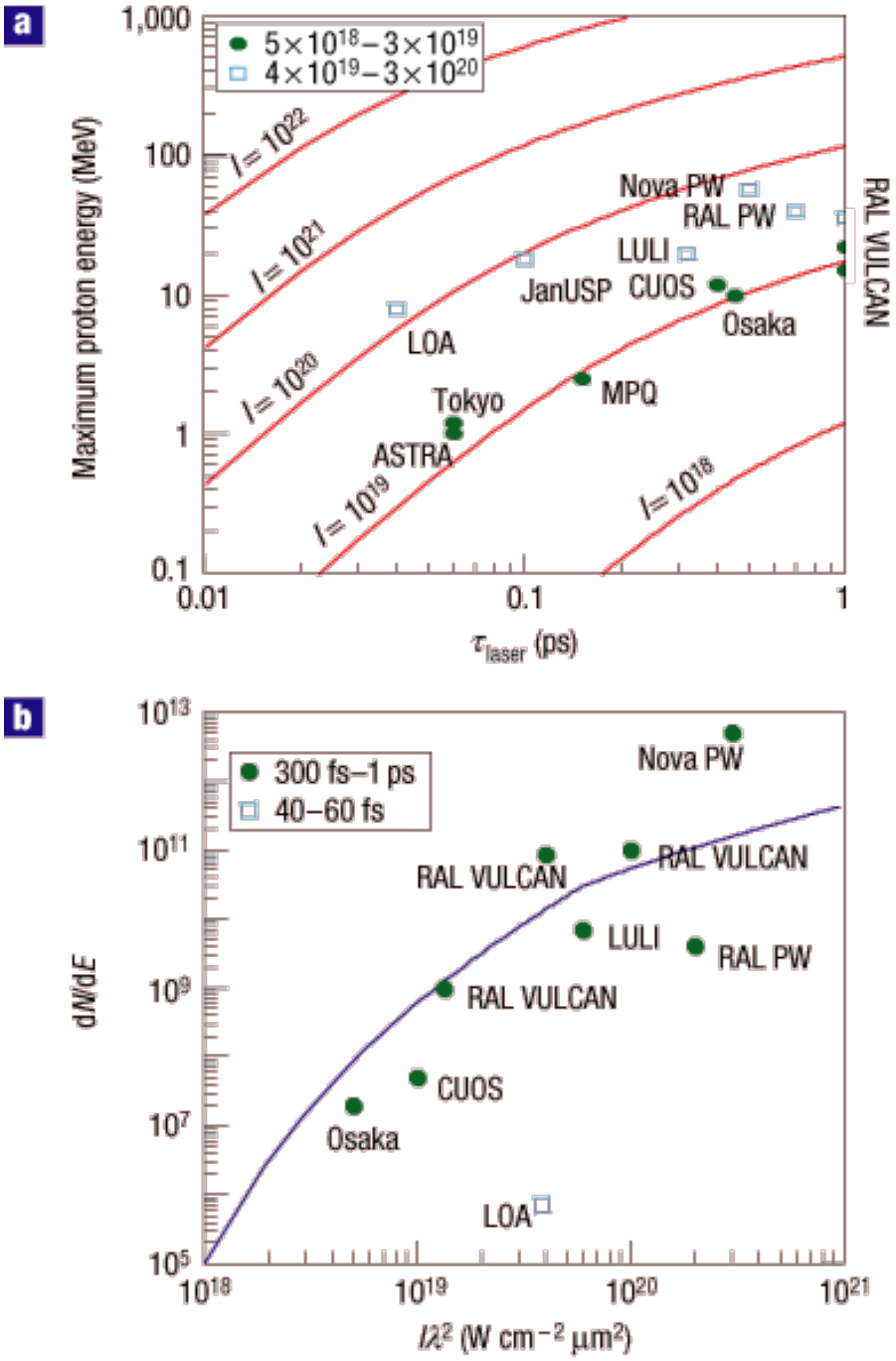


Figure 4.4: Calculations using the fluid model (assuming 20 μm-thick targets, a 10 μm FWHM laser spot size and a 0.5 ps laser pulse duration) and experimental data (circles and squares). (a) Maximum proton energy as a function of laser pulse duration. The intensities are in units of $\mathrm{W\,cm^{-2}}$. (b) Number of protons in a 1 MeV bin around 10 MeV as a function of laser intensity multiplied by the laser wavelength squared. The last parameter is chosen as it governs the hot electron temperature. Figures taken from [10].

# Chapter 5

# Numerical Results

We now estimate the number of neutrons that would be produced in the experimental setup described in the introduction. We calculate this for different laser power, intensity and pulse duration and also vary the thickness of the primary target and the temperature of the secondary target. Fix parameters are the laser wavelength $\lambda = 800$ nm as well as the thickness $d_D = 10$ μm and density $n_D = 10^{21}$ cm$^{-3}$ of the deuteron target.

First, we use Eq. (4.17) to calculate the energy spectrum of the lithium ions as they leave the primary target. The spectrum for one set of laser parameters is shown in Fig. 5.1. The different cut-off energies as calculated via Eq. (4.12) are listed in Table 5.2.

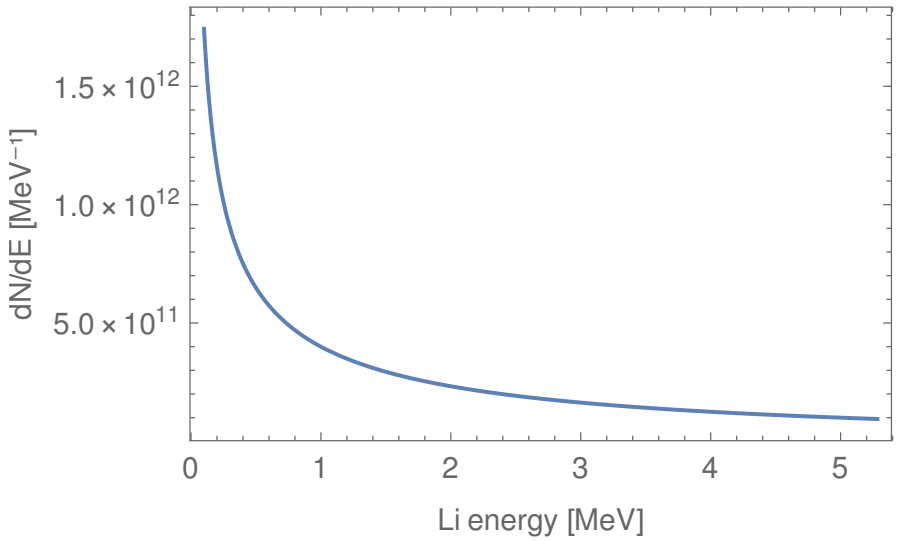


Figure 5.1: Spectrum of lithium ions as function of the lithium energy for the parameter set no.2 in Table (5.2)

.

## 5.1 Nuclear cross section data

In order to calculate the reaction rate, we need the data of the cross section for the reaction $^7$Li(d,n)2$^4$He. For very low energies there are no measurements of the cross section itself but extrapolations of the astrophysical S-factor, which then give the cross section via Eq. (3.8). For the energy range $E \leq 0.05$ MeV we take from Ref. [19]

$$S(E) = 80 \text{ mbMeV} - 37\text{mb} \cdot E$$

and from Ref. [12] for $0.05 \text{ MeV} < E \leq 0.10$ MeV the S-factor

$$S(E) = 151 \text{ mbMeV} - 1020\text{mb} \cdot E.$$

The cross section in the range $0.104 \text{ MeV} \leq E < 1.68$ MeV, $0.477 \text{ MeV} \leq E < 3.806$ MeV and $2.15 \text{ MeV} \leq E < 8.524$ MeV was measured in Refs. [3], [21] and [16], respectively. The data given in Ref. [21] and Ref. [3] are the differential cross section per solid angle at only one specific angle, so that the approximation $\sigma \approx 4\pi d\,\sigma/d\Omega$ has to be used. According to Ref. [19], this is a reasonable assumption for low energies. For high energies, however, this approximation seems to highly overestimate the cross section, comparing to the result in Ref. [16]. We therefore use the cross section given in Ref. [3] for $0.104 \text{ MeV} \leq E < 0.477$ MeV and the mean value of the measurements in Ref. [3] and Ref. [3] for $0.477 \text{ MeV} \leq E < 1.68$ MeV and finally the data from Ref. [16] for high energies $2.15 \text{ MeV} \leq E < 8.52$ MeV. The interpolation of these values is shown in Fig. 5.2.
One can observe two resonances at $E \approx 800$MeV and $E \approx 600$MeV. We assume that these resonances correspond to the excited levels $J^\pi = \frac{7}{2}^+$ and $J^\pi = \frac{5}{2}^-$ of $^9$Be. The mass difference is

$$Q = m(^9\text{Be}) - m(^7\text{Li}) - m(\text{D}) = 16.69 \text{ MeV}.$$

The sum of the Q-value and the center-of-mass energy of the reaction at the observed resonances therefore equals the energies of these two exited states, which are given as $17.495 \pm 0.005$ MeV and $17.300 \pm 0.005$ MeV in Ref. [2].

## 5.2 Neutron Number

In our one-dimensional model the center-of-mass energy is

$$E = \frac{1}{2}\mu\left(\sqrt{\frac{2}{m_{Li}}E_{Li}} - v_D\right)^2, \tag{5.1}$$

and the deuteron velocity follows a Gaussian distribution

$$\Phi = \left(\frac{1}{2\pi}\right)^{\frac{1}{2}} \exp\left(-\frac{\tilde{v}_D^2}{2}\right), \tag{5.2}$$

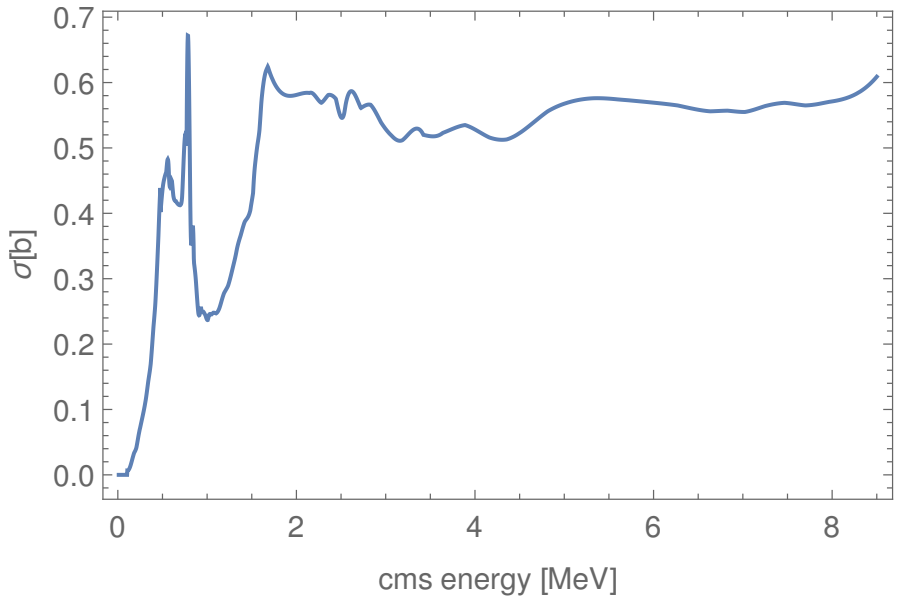


Figure 5.2: Cross section of $^7$Li(d,n)2$^4$He in the center-of-mass system.

where $\tilde{v}_D = v_D/\sqrt{k_B T/m_D}$ is the deuteron velocity normed by the standard deviation $\sqrt{k_B T/m_D}$ in thermal equilibrium. The disrtribution is normed to one

$$\int_{-\infty}^{\infty} \Phi(\tilde{v}_D)\,\mathrm{d}\tilde{v}_D = 1. \tag{5.3}$$

We average the cross section at a given lithium ion energy over all deuteron velocities between ±5 standard deviations to find the mean cross section,

$$< \sigma > (E_{Li}) = \int_{-5}^{5} \sigma(E)\Phi(\tilde{v}_D)\,\mathrm{d}\tilde{v}_D. \tag{5.4}$$

The number of neutrons $N_n$ per unit lithium energy is then given by the product of the lithium spectrum with the area density $n_D d_D$ of the deuterons and the mean cross section

$$\frac{dN_n}{dE_{Li}} = \frac{dN_{Li}}{dE_{Li}} \cdot n_D d_D \cdot < \sigma > (E_{Li}). \tag{5.5}$$

We finally calculate the total number of neutrons in the reaction by integrating the spectrum given in Eq. (5.5) over all lithium energies from 0 to the cut-off energy [see Eq. (4.12)]. To account for the electron screening effect in the plasma this result has to be multiplied by the screening factor $g_{scr}$ from Eq. (3.33). As can be seen in Table 5.1 and Fig. 5.3, this screening factor is negligibly different from 1 for high temperatures.

In the second scenario, where the reaction does not take place in plasma but in the gas target, the deuterons are cold enough to neglect the deuteron velocity $v_D$. Thus, the averaged cross section in Eq. (5.5) is replaced by the cross section at center-of-mass energy $E = \frac{1}{2}\mu/m_{Li}E_{Li}$. The lower deuteron velocity in gases causes the difference between the neutron numbers in plasma compared to gas at high

| T [eV] | 100 | $10^4$ | $10^5$ |
|---|---|---|---|
| density [ $cm^{-3}$ ] | $10^{21}$ | $10^{21}$ | $10^{21}$ |
| screening factor | 1.02633 | 1 | 1 |

Table 5.1: Screening factor at given deuteron temperature and density

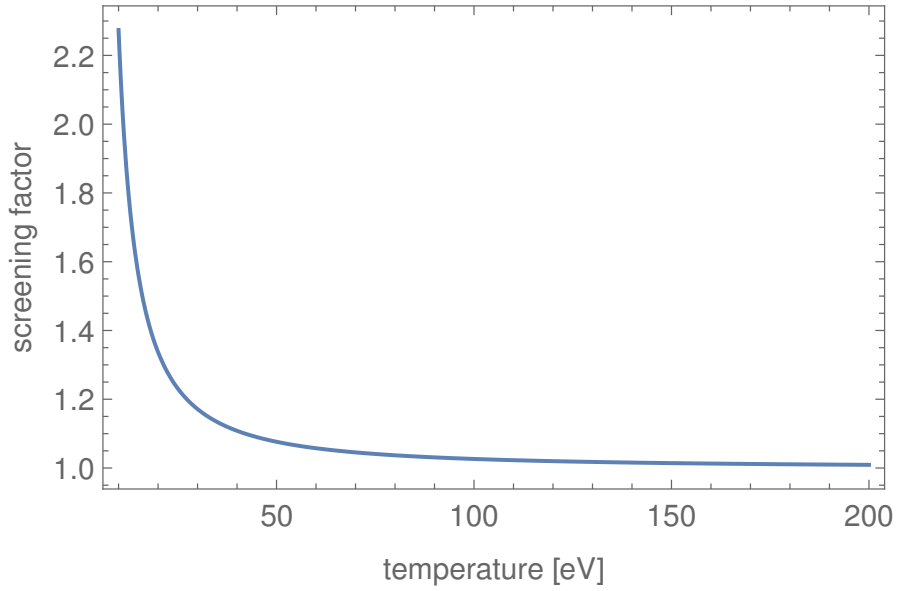


Figure 5.3: Calculated screening factor as a function of the plasma temperature.

plasma temperatures where the electron screening has no effect on the result [see Table 5.2]. These differences are small, however, since the deuteron velocities are relatively small compared to the lithium velocity even at high temperatures.

At low temperature (100 eV), where the screening is the strongest, the screening effect is still relatively weak, causing only a difference of 2% between the neutron numbers in gas compared to plasma (see Table 2.1).

The neutron spectra, both for reactions in plasma and in gas for several laser and target parameter, are shown in Fig.5.4 to 5.13. One can see that the higher the temperature in which the reaction takes place, the more washed out are the features of the spectrum. In particular, all the spectra in gas show several local maxima that do not occur in the corresponding spectrum for plasma. This is because at higher temperature the deuterons reach higher velocities so that at each lithium energy a broader range of center-of-mass energies of the reaction are possible. The local maxima of the center-of-mass cross section given in Fig. 5.3 are thus washed out when the average in Eq. (5.4) is taken.

As can bee seen in Table 5.2 the highest number of neutrons is achieved with parameter set no. 7. This is due to the high laser puls length which causes a high TNSA cut-off energy and thus a high center-of-mass energy in the reaction, corresponding to a high cross section.
From parameter sets 1-3 one can see that the neutron number increases with decreasing thickness of the primary target. A thicker target yields more hot electrons under laser irradiation so that higher ion energies are reached through the TNSA mechanism. The optimal value for the target thickness, at which the TNSA process leads to the highest ion energies, depends on the prepulse duration, as has been

investigated experimentally [13]. For very thin targets a prepulse-induced plasma formation at the rear side effectively suppresses TNSA.

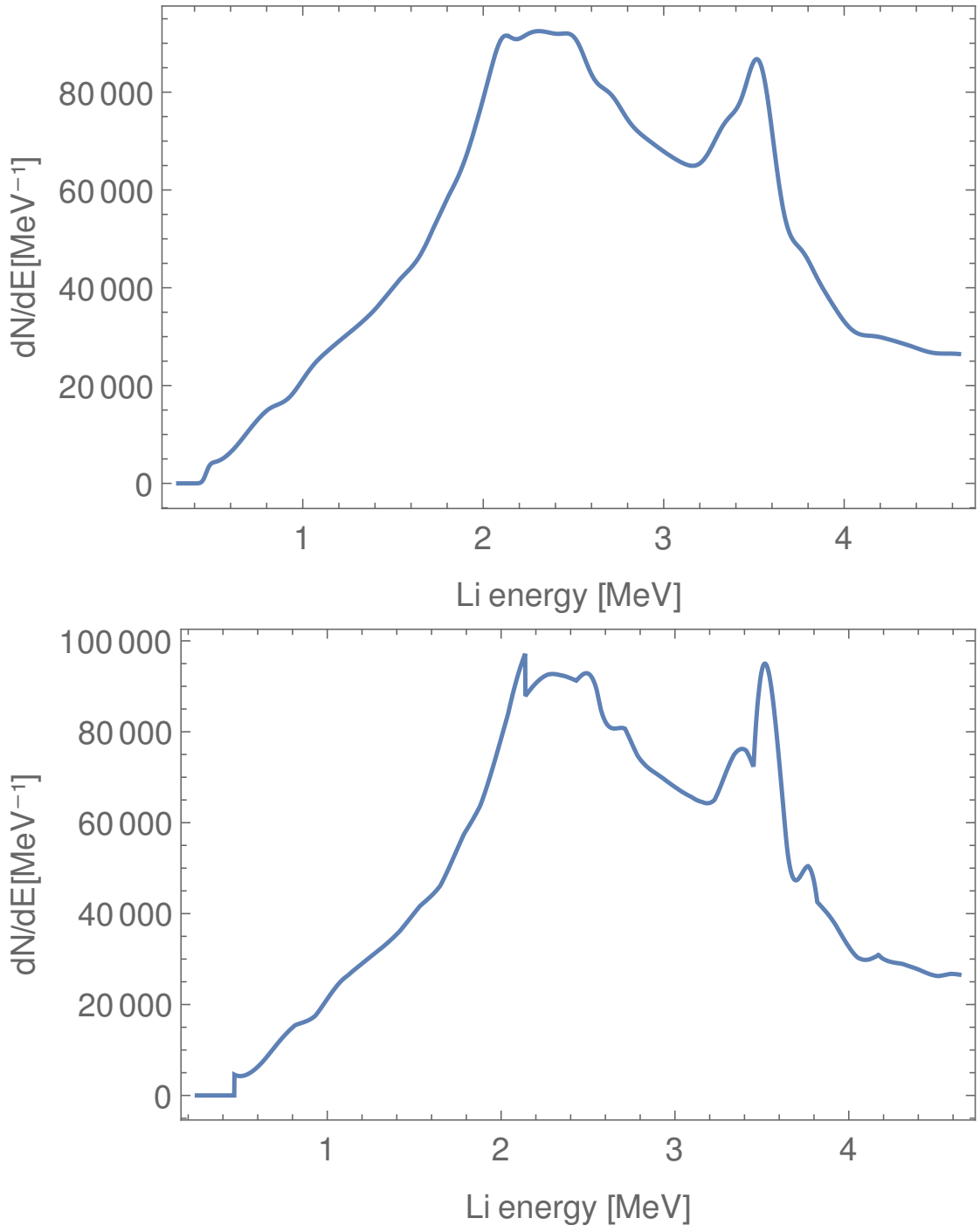


Figure 5.4: Neutron spectrum for parameter set no. 1 for reaction in plasma (top) or gas (bottom)

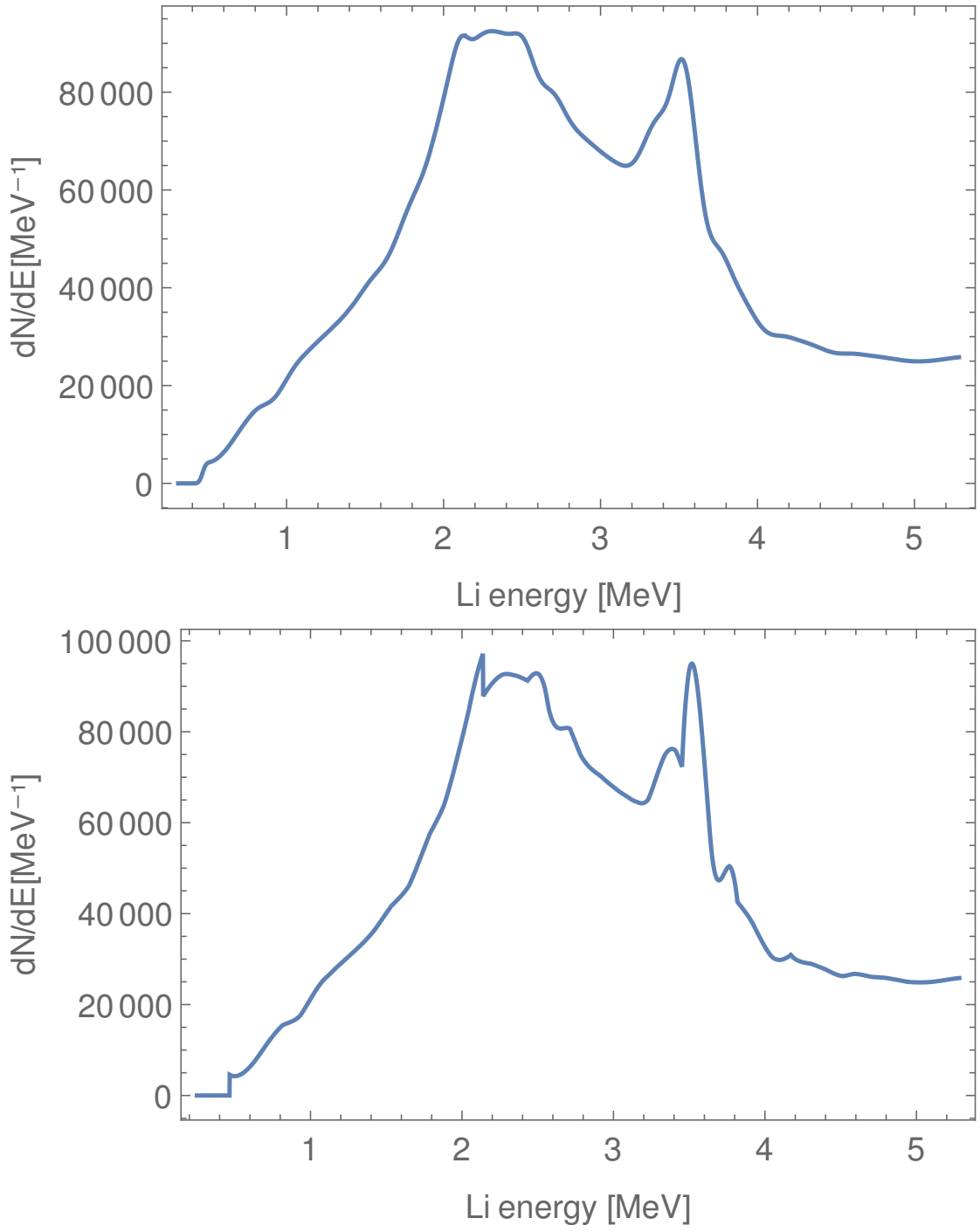


Figure 5.5: Neutron spectrum for parameter set no. 2 for reaction in plasma (top) or gas (bottom)

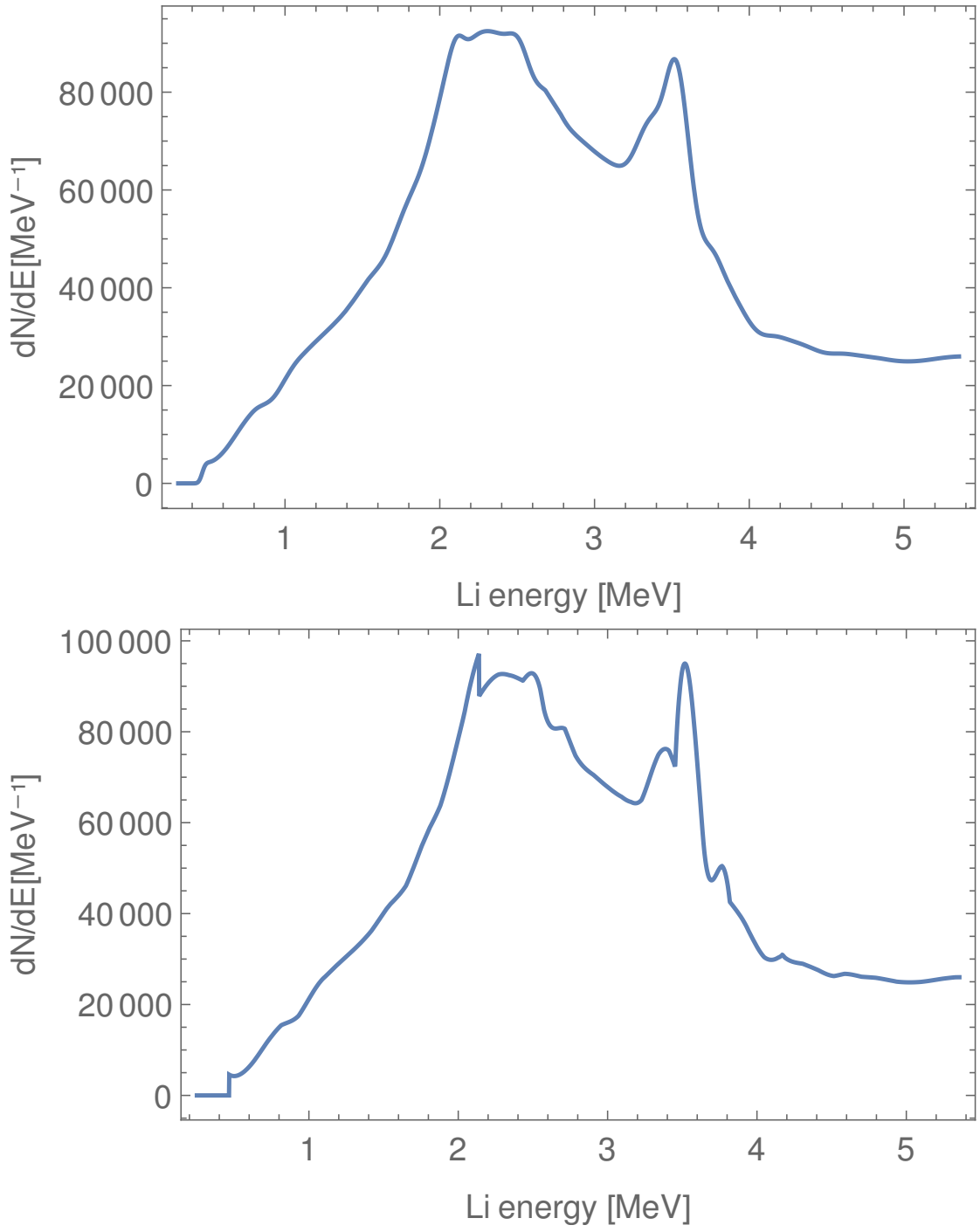


Figure 5.6: Neutron spectrum for parameter set no. 3 for reaction in plasma (top) or gas (bottom)

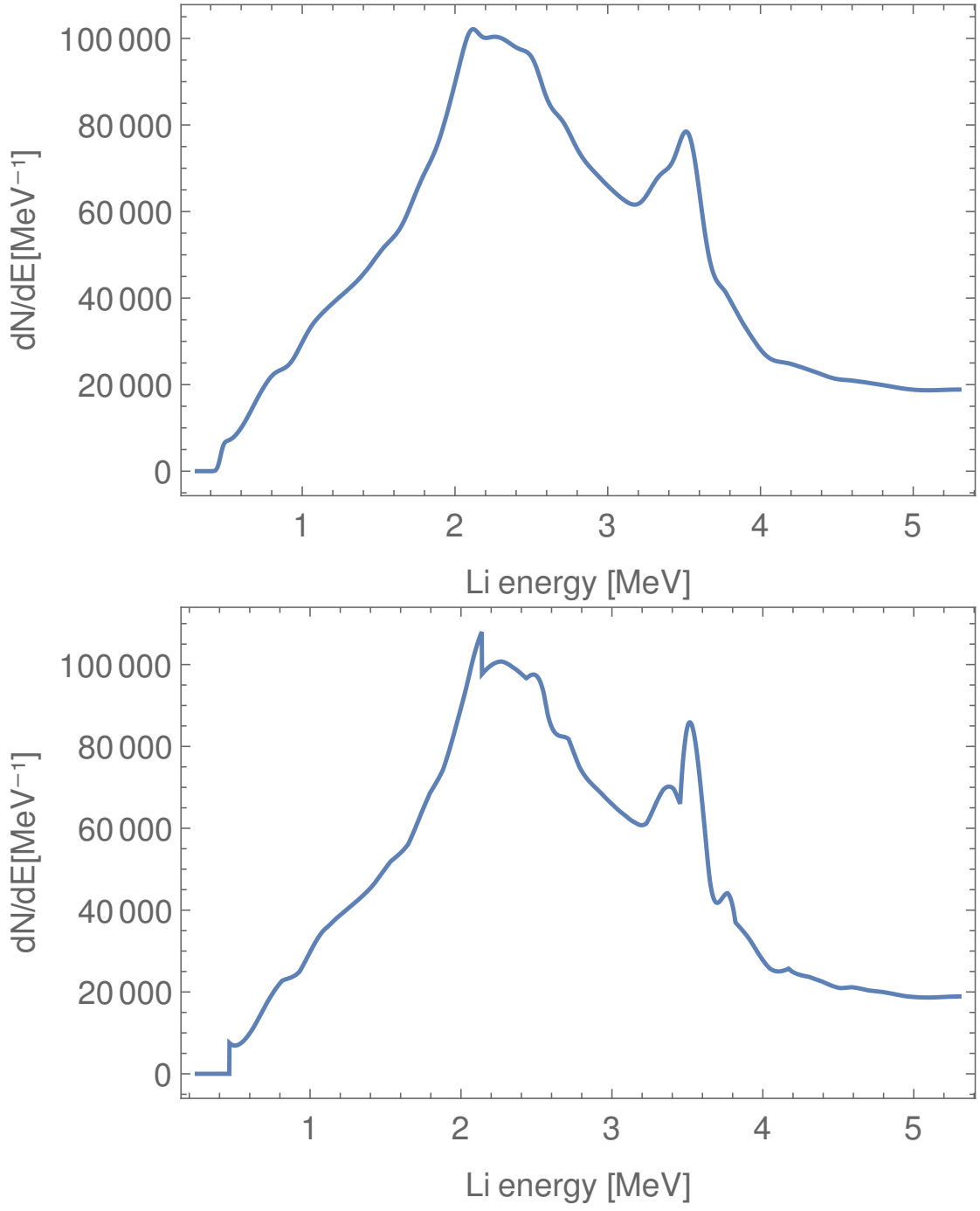


Figure 5.7: Neutron spectrum for parameter set no. 4 for reaction in plasma (top) or gas (bottom)

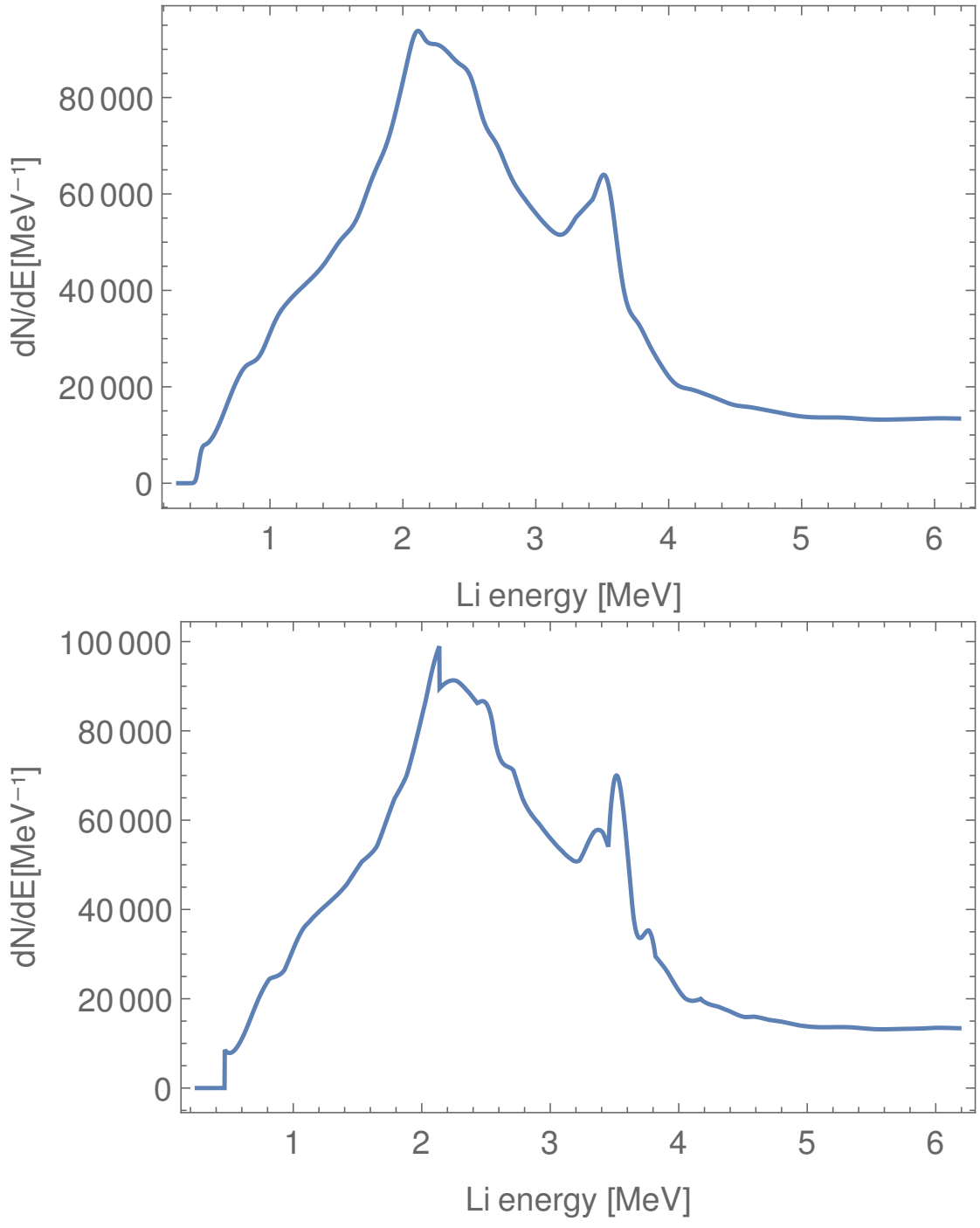


Figure 5.8: Neutron spectrum for parameter set no. 5 for reaction in plasma (top) or gas (bottom)

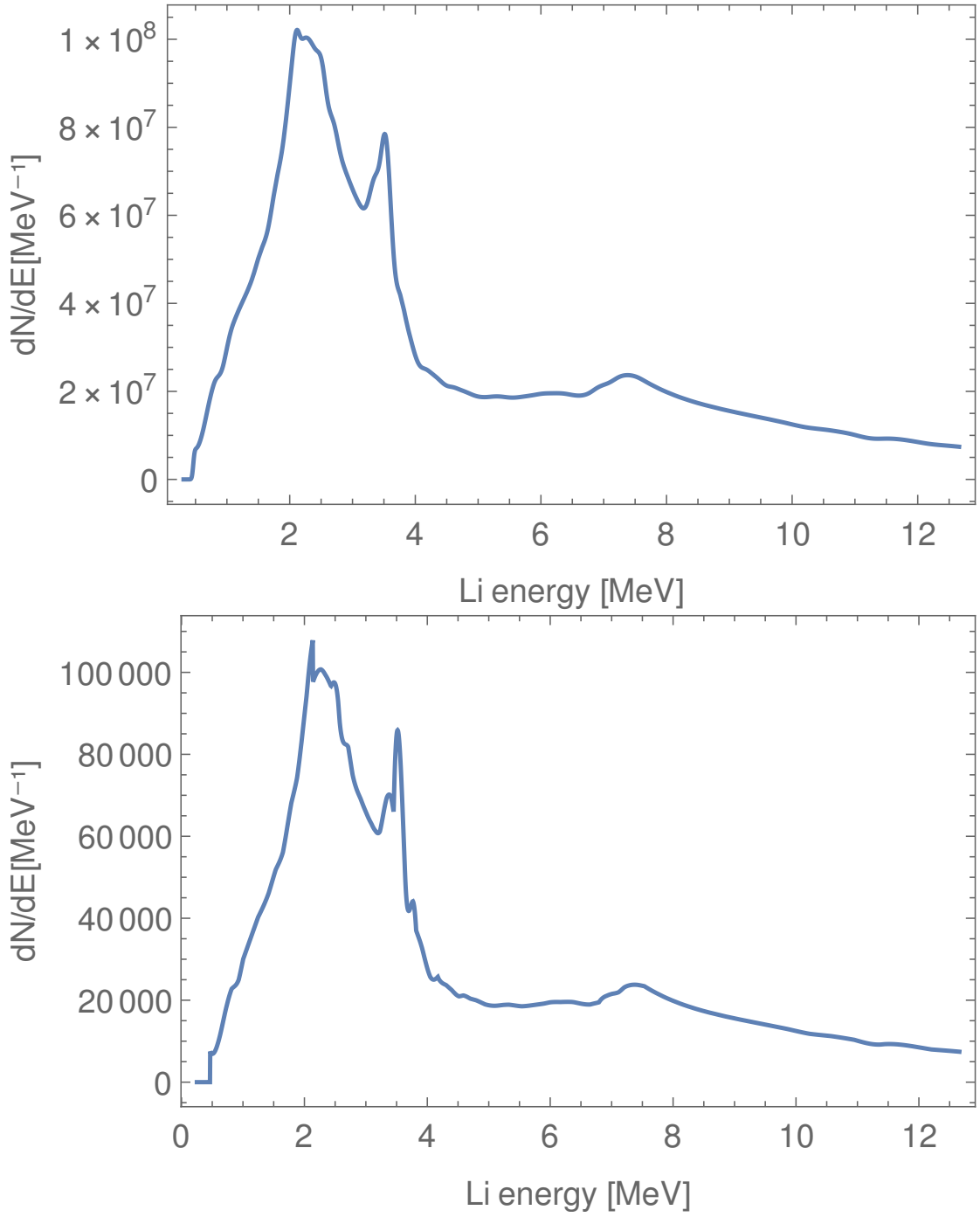


Figure 5.9: Neutron spectrum for parameter set no. 6 for reaction in plasma (top) or gas (bottom)

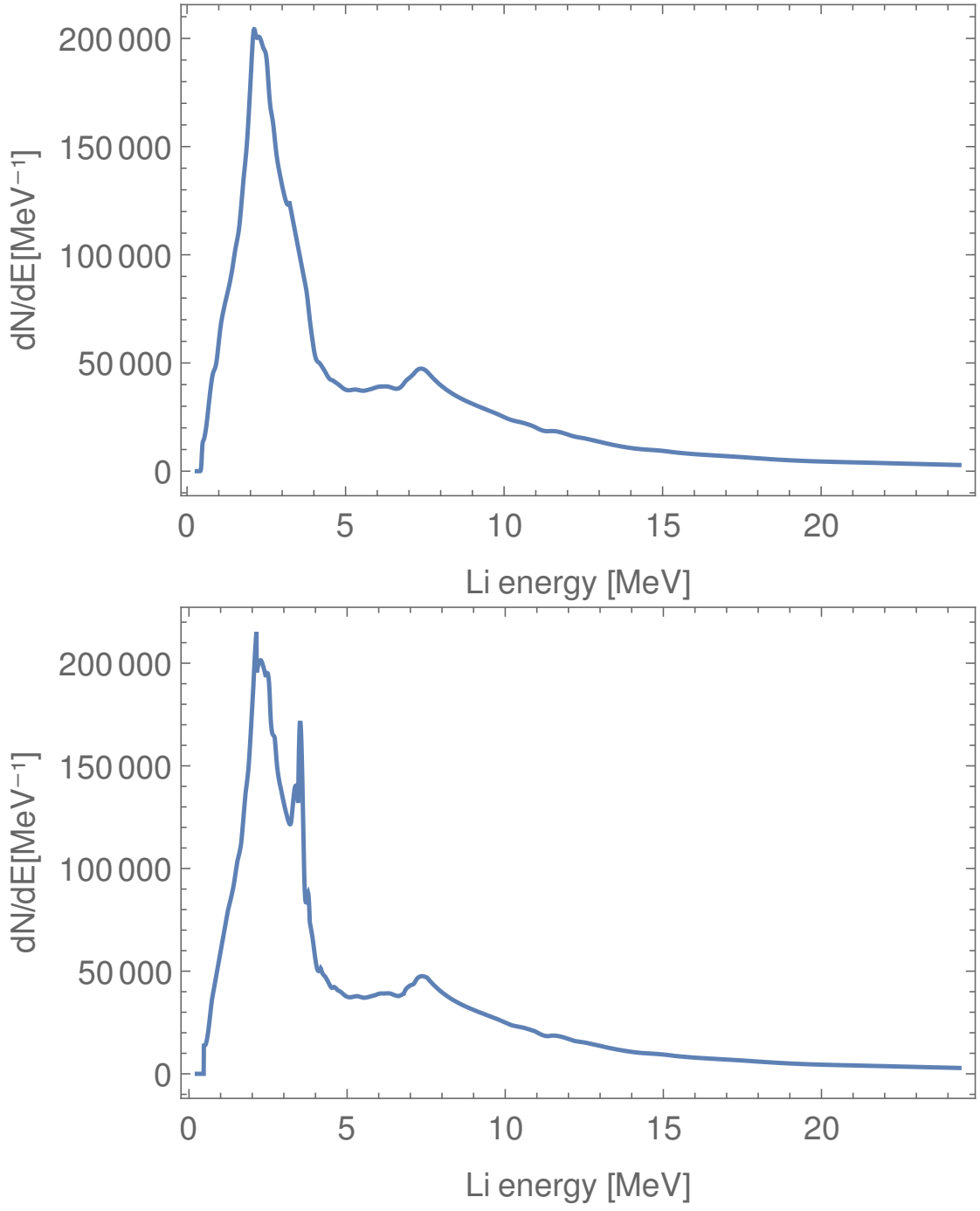


Figure 5.10: Neutron spectrum for parameter set no. 7 for reaction in plasma (top) or gas (bottom)

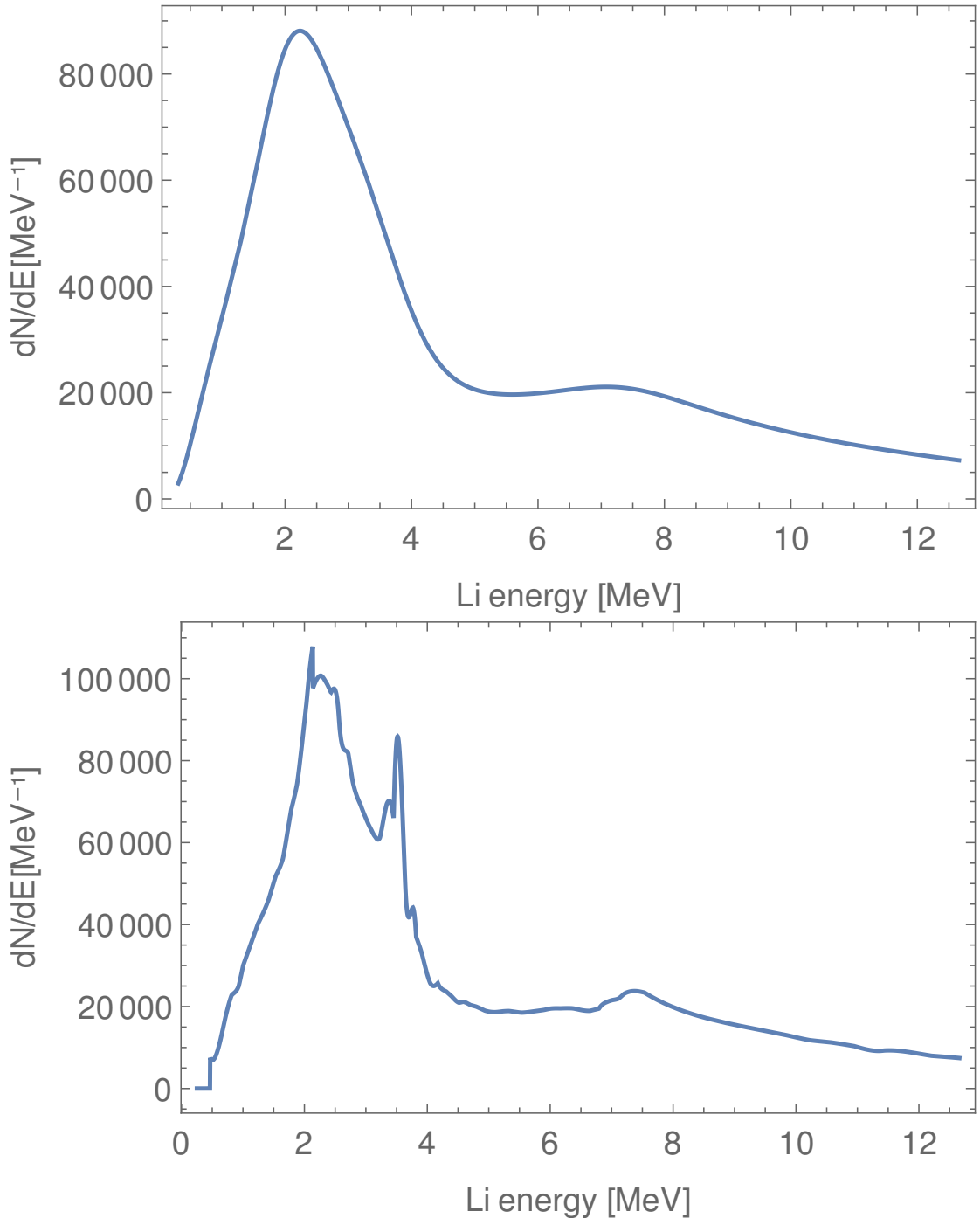


Figure 5.11: Neutron spectrum for parameter set no. 8 for reaction in plasma (top) or gas (bottom)

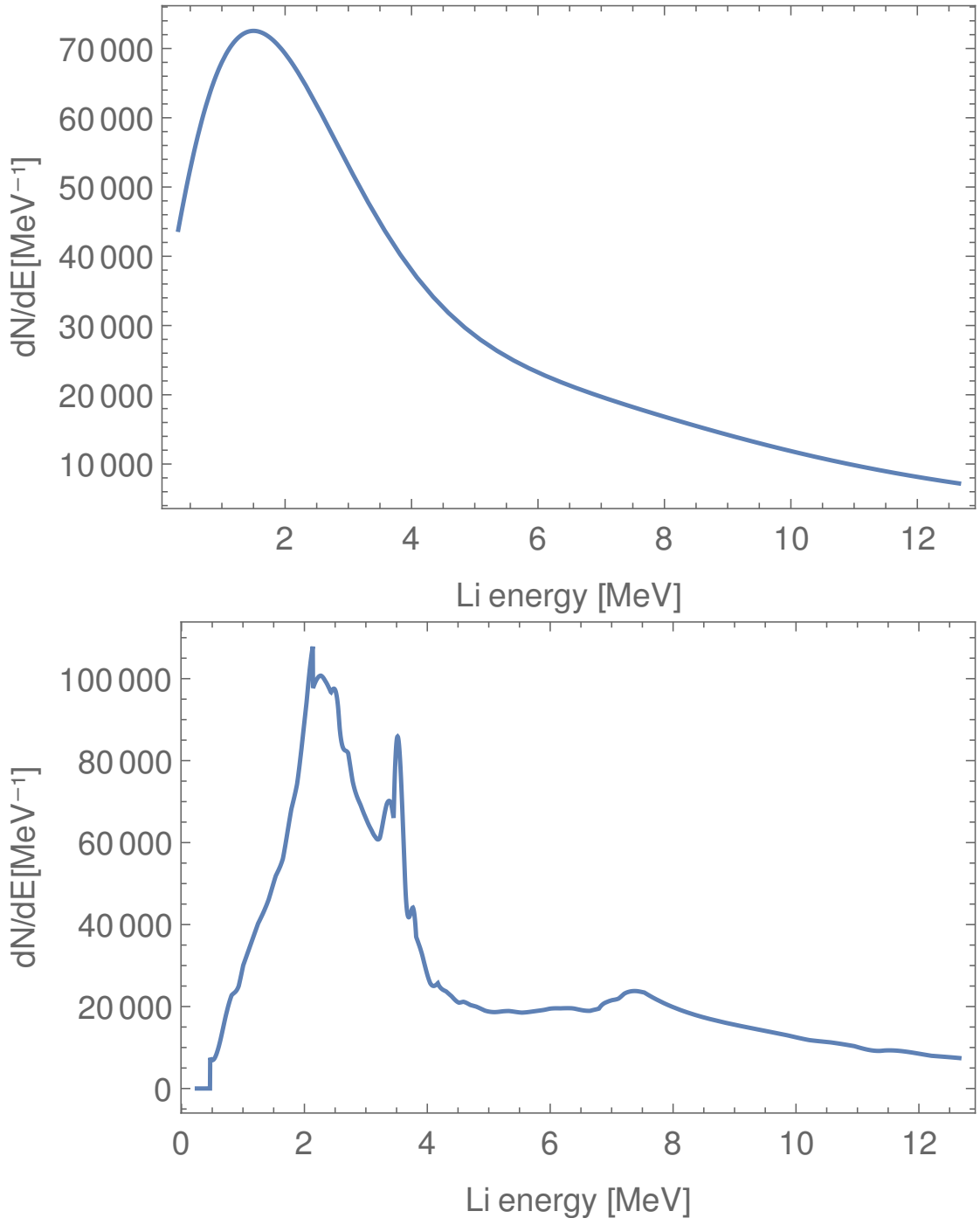


Figure 5.12: Neutron spectrum for parameter set no. 9 for reaction in plasma (top) or gas (bottom)

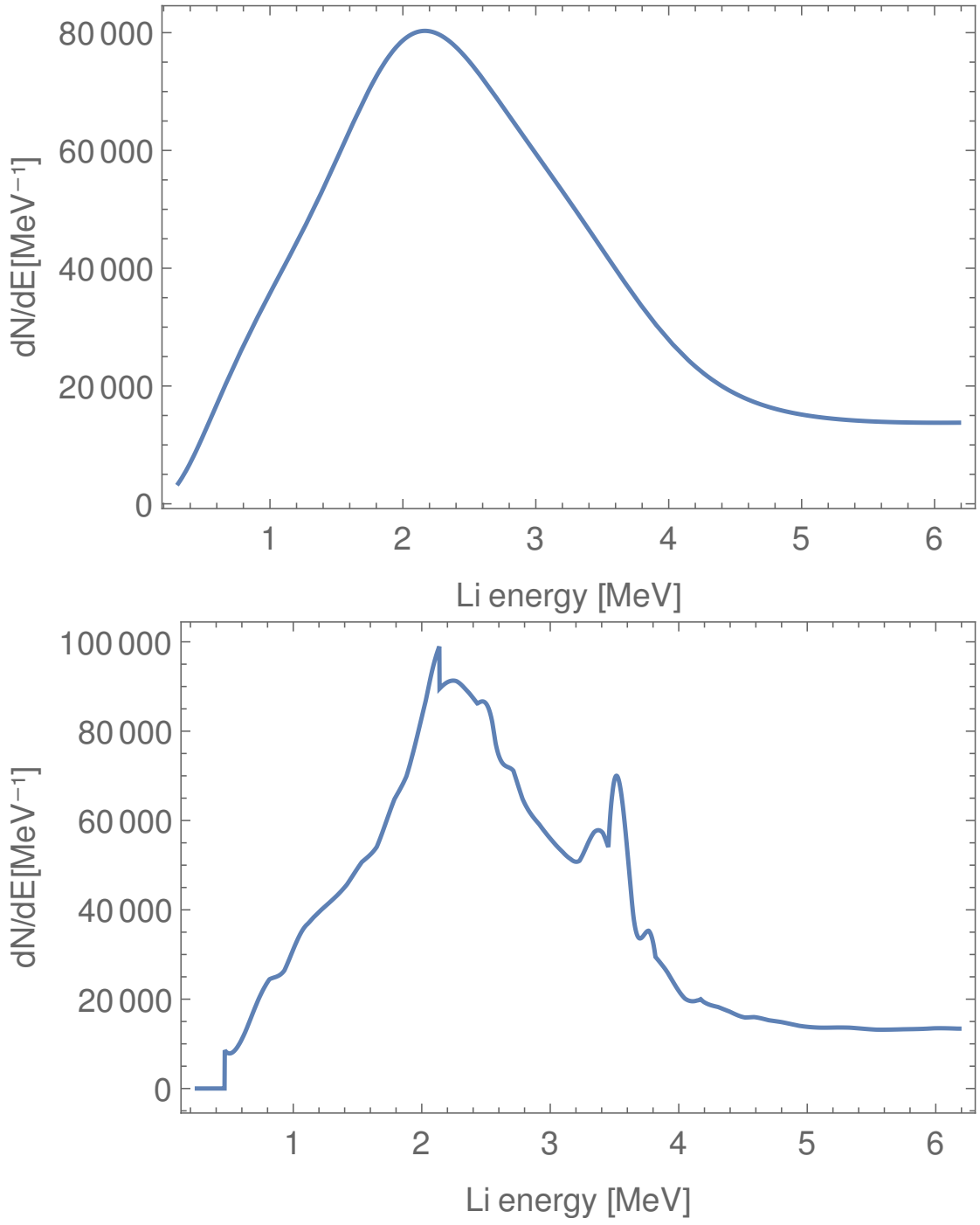


Figure 5.13: Neutron spectrum for parameter set no. 10 for reaction in plasma (top) or gas (bottom)

| Parameter set | 1 | 2 | 3 | 4 | 5 | 6 | 7 | 8 | 9 | 10 |
|---|---|---|---|---|---|---|---|---|---|---|
| laser power $P$[ PW] | 10 | 10 | 10 | 2 | 1 | 1 | 1 | 1 | 1 | 1 |
| laser intensity $I$[ W cm$^{-2}$] | $10^{20}$ | $10^{20}$ | $10^{20}$ | $10^{19}$ | $5 \cdot 10^{18}$ | $10^{19}$ | $10^{19}$ | $10^{19}$ | $10^{19}$ | $5 \cdot 10^{18}$ |
| laser pulse duration $\tau$[ fs] | 25 | 25 | 25 | 125 | 250 | 250 | 500 | 250 | 250 | 250 |
| deuteron temperature $T[eV]$ | 100 | 100 | 100 | 100 | 100 | 100 | 100 | $10^4$ | $10^5$ | $10^4$ |
| thickness of primary target $d_t$[ $\mu$m] | 10 | 1 | 0.1 | 1 | 1 | 1 | 1 | 1 | 1 | 1 |
| cut-off energy[ MeV] | 4.64 | 5.28 | 5.36 | 5.30 | 6.18 | 12.66 | 24.36 | 12.66 | 12.66 | 6.18 |
| neutrons (plasma)[$10^5$] | 2.19610 | 2.36545 | 2.38454 | 2.41977 | 2.25897 | 3.57300 | 7.92126 | 3.51285 | 3.81531 | 2.20102 |
| neutrons (gas) [$10^5$] | 2.13965 | 2.30451 | 2.32317 | 2.35731 | 2.20057 | 3.48102 | 7.71665 | 3.48102 | 3.48102 | 2.20057 |

Table 5.2: Number of neutrons for reactions in plasma or gas and TNSA cut-off energy.

# Chapter 6

# Summary and outlook

We have described a possible experimental setup that can be used to measure reaction rates under extreme plasma conditions by colliding two plasmas making use of the TNSA mechanism. The goal of this thesis was to give an estimation of the number of neutrons that the $^{7}$Li(d,n)2$^{4}$ reaction would produce in such an experiment.
In order to do that, we have used an one-dimensional, isothermal, fluid model of plasma expansion into vacuum to describe the TNSA process and thereby find the lithium ion energy that would be achieved in the experiment. For the reaction rate the effect of electron screening had to be considered. Given the high temperature of the plasma the Coulomb interaction energy between a nucleus and the and the nearest few electrons and nuclei is small compared to the thermal energy and the screening therefore weak. This has simplified the theoretical description of the screening factor. We have then used this screening factor and the cross section from experimental data to find the number of neutrons for the cases that the reaction takes place in plasma or in gas.

The results show that the electron screening affects the neutron yield by no more than 2%. We conclude that the $^{7}$Li(d,n)2$^{4}$ reaction is not well suited to experimentally study the effects of plasma screening for nuclear reactions in astrophysical environments. However, the calculated neutron yields for this reaction show that the experimental determination of the cross section in a plasma environment is possible with currently available laser parameters. This would be the first time that one can reproduce in the laboratory astrophysical plasma conditions. As an outlook, other nucleosynthesis-relevant reactions that are more sensitive to the screening effect in plasmas could be investigated.

# Bibliography


[1] Stefano Atzeni and Jürgen Meyer ter Vehn. *The Physics of Inertial Fusion*. Oxford Science Publications, 2004.

[2] G. Audi, A.H. Wapstra, and C. Thibault. The ame2003 atomic mass evaluation. *Nuclear Physics A*, 729(1):337 – 676, 2003.

[3] L. M. Baggett and S. J. Bame. The disintegration of lithium by deuteron bombardment. *Phys. Rev.*, 85:434–436, Feb 1952.

[4] R. N. Boyd, C. A. Mitchell, and B. S. Meyer. Reaction rate for destruction of $^7$Li and primordial nucleosynthesis. *Phys. Rev. C*, 47:2369–2373, May 1993.

[5] Alain Coc, Stéphane Goriely, Yi Xu, Matthias Saimpert, and Elisabeth Vangioni. Standard big bang nucleosynthesis up to cno with an improved extended nuclear network. *The Astrophysical Journal*, 744(2):158, 2012.

[6] Richard H. Cyburt, Brian D. Fields, Keith A. Olive, and Tsung-Han Yeh. Big bang nucleosynthesis: Present status. *Rev. Mod. Phys.*, 88:015004, Feb 2016.

[7] J R Davies. Laser absorption by overdense plasmas in the relativistic regime. *Plasma Physics and Controlled Fusion*, 51(014006), 2009.

[8] Brian D. Fields. The primordial lithium problem. *Annual Review of Nuclear and Particle Science*, 61:47, 2011.

[9] F.Negoita et al. Laser driven nuclear physics at eli-np. *Romanian Reports in Physics*, 68:37–144, 2015.

[10] J. Fuch et al. Laser-driven proton scaling laws and new paths towards energy increase. *Nature Physics*, 2:48–54, 2006.

[11] M. C. Levy et al. Petawatt laser absorption bounded. *Nature Communication*, 5(4149), 2014.

[12] F.E. Cecil J.A. McNeil C.S. Galovich M.A. Hoffstee, A.K. Pallone. Measurement of low energy (d,n) reactions on light nuclei important to astrophysics. *Nuclear Physics A*, 688:527c–529c, 2001.

[13] Andrea Macchi, Marco Borghesi, and Matteo Passoni. Ion acceleration by superintense laser-plasma interaction. *Rev. Mod. Phys.*, 85:751–793, May 2013.

[14] G. Malka and J. L. Miquel. Experimental confirmation of ponderomotive-force electrons produced by an ultrarelativistic laser pulse on a solid target. *Phys. Rev. Lett.*, 77:75–78, Jul 1996.

[15] P. Mora. Plasma expansion into a vacuum. *Phys. Rev. Lett.*, 90:185002, May 2003.

[16] C. Nussbaum. Energy dependences of total cross sections of neutron formation in reactions li-6,7 + h-2,3. *Prikladnaya Yadernaya Spektroskopiya (Applied Nuclear Spectroscopy)*, 13:135, 1984.

[17] M. Passoni and M. Lontano. Theory of light-ion acceleration driven by a strong charge separation. *Phys. Rev. Lett.*, 101:115001, Sep 2008.

[18] Rodney Rolfs. *Cauldrons in the Cosmos*. University of Chicago, 1988.

[19] A. Sabourov, M. W. Ahmed, M. A. Blackston, A. S. Crowell, C. R. Howell, B. A. Perdue, K. Sabourov, A. Tonchev, H. R. Weller, R. M. Prior, and M. C. Spraker. Astrophysical $S$ factor for the $^7\mathrm{Li}(d,n_0)^8\mathrm{Be}$ and $^7\mathrm{Li}(d,n_1)^8\mathrm{Be}$ reactions. *Phys. Rev. C*, 73:015801, Jan 2006.

[20] E. E. Salpeter. Electrons screening and thermonuclear reactions. *Australian Journal of Physics*, 7:373–388, 1954.

[21] J. C. Slattery, R. A. Chapman, and T. W. Bonner. Excited states in be$^7$ and be$^8$. *Phys. Rev.*, 108:809–811, Nov 1957.

[22] R. P. Town et al. Experimental confirmation of ponderomotive-force electrons produced by an ultrarelativistic laser pulse on a solid target. *Nucl. Instrum. Methods Phys. Res. A*, 544(61), 2005.

[23] S. C. Wilks, W. L. Kruer, M. Tabak, and A. B. Langdon. Absorption of ultra-intense laser pulses. *Phys. Rev. Lett.*, 69:1383–1386, Aug 1992.

# Acknowledgments

I wish to thank my supervisor PD Adriana Palffy for her help, in particular in the stressful end phase of writing this thesis.

I would also like to offer my special thanks to Yuanbin Wu for giving me access to his code on the Carbon-Helium reaction and his useful advice throughout my work on this thesis.

# Erklärung

Ich versichere, dass ich diese Arbeit selbstständig verfasst und keine anderen als die angegebenen Quellen und Hilfsmittel benutzt habe.

Heidelberg, den